https://doi.org/10.5194/essd-2026-531
Preprint. Discussion started: 10 August 2026

A Gauge-Based Monthly Natural Discharge Reconstruction Dataset for the Eurasian Arctic, 1952–2025

Bingshi Liu[1,2,*], Xiancai Zou[1,2], Jiancheng Li[1,2,3], and Taoyong Jin[1,2]

[1] School of Geodesy and Geomatics, Wuhan University, Wuhan, China

[2] Key Laboratory of Geospace Environment and Geodesy, Ministry of Education, Wuhan University, Wuhan, China

[3] School of Geosciences and Info-Physics, Central South University, Changsha, China

Correspondence to: Bingshi Liu (bs.liu@whu.edu.cn).

Abstract. River discharge provides one of the clearest measures of how Arctic freshwater systems respond to climate change, yet long-term and continuous monitoring remains challenging. Here we present a gauge-based monthly natural discharge reconstruction dataset for 94 gauging stations in the Eurasian Arctic from 1952 to 2025. The dataset was generated using a basin-scale framework driven by precipitation and air temperature and aided by snow information. Terrestrial water storage (TWS) serves as the key link in the framework. Historical TWS was first reconstructed using an improved state-update empirical model constrained by TWS observations from the Gravity Recovery and Climate Experiment (GRACE), and monthly natural discharge was then estimated from reconstructed TWS using a refined runoff–TWS relationship calibrated against gauge discharge observations. The reconstructed monthly natural discharge agreed well with observations at minimally regulated gauges and during pre-regulation periods at regulated gauges, with median monthly Kling–Gupta efficiency (KGE) values exceeding 0.88. When monthly values were aggregated to annual discharge, the reconstruction still captured observed variability at minimally regulated gauges, with a median annual KGE of 0.73. The dataset generally agreed better with gauge observations than discharge estimates derived from existing GRACE-like TWS products and an existing gridded runoff reconstruction product. Example applications illustrate spatially heterogeneous trends in annual discharge and seasonal allocation over the past seven decades and show how the dataset can be used to assess the effects of human regulation on river discharge. This dataset provides a long-term natural-discharge baseline for characterizing historical discharge variability and assessing the roles of climate variability and human regulation in poorly monitored Arctic basins. The reconstructed monthly natural discharge dataset is available at https://doi.org/10.5281/zenodo.21157816 (Liu et al., 2026).

1 Introduction

The Arctic is warming rapidly, with widespread effects on the regional hydrological cycle (Box et al., 2019; Bring et al., 2016; Winkelbauer et al., 2022). The Eurasian Arctic, home to large rivers such as the Ob, Yenisey, and Lena, contributes approximately two-thirds of the total pan-Arctic river discharge to the Arctic Ocean (Feng et al., 2021). Observations have shown a marked increase in freshwater discharge from Eurasian rivers to the Arctic Ocean during recent decades (Feng et al., 2021; Gudmundsson et al., 2025; Peterson et al., 2002). River discharge integrates changes in basin-scale precipitation, evapotranspiration, and terrestrial water storage (TWS; An index of abbreviations is provided in Table S1). Its continuous monitoring, therefore, provides one of the most direct observational means of identifying how the Arctic freshwater system responds to climate change (Holmes, 2021; White et al., 2007).

Despite this need, discharge observations in the Eurasian Arctic remain temporally discontinuous and spatially uneven. Among the 94 gauging stations compiled in this study (Figure 1a), even in the 1980s, the period with the highest data coverage, the overall availability of monthly discharge records across all gauges was only approximately 85% (Figure 1b). The proportion of gauges

https://doi.org/10.5194/essd-2026-531
Preprint. Discussion started: 10 August 2026

with annual record completeness above 90% was lower, remaining close to 80% only between 1977 and 1989 (Figure 1b). After the early 1990s, the number of active stations and available records declined markedly, partly reflecting reduced monitoring capacity and limited data sharing (Bring and Destouni, 2014; Feng et al., 2021; Shiklomanov et al., 2002). Recent continuous records are largely limited to major rivers and downstream gauges, leaving many tributaries and smaller rivers poorly monitored (Figure 1c). Consequently, gauge observations alone cannot fully quantify Eurasian freshwater export to the Arctic Ocean, and substantial ungauged contributions must be estimated.

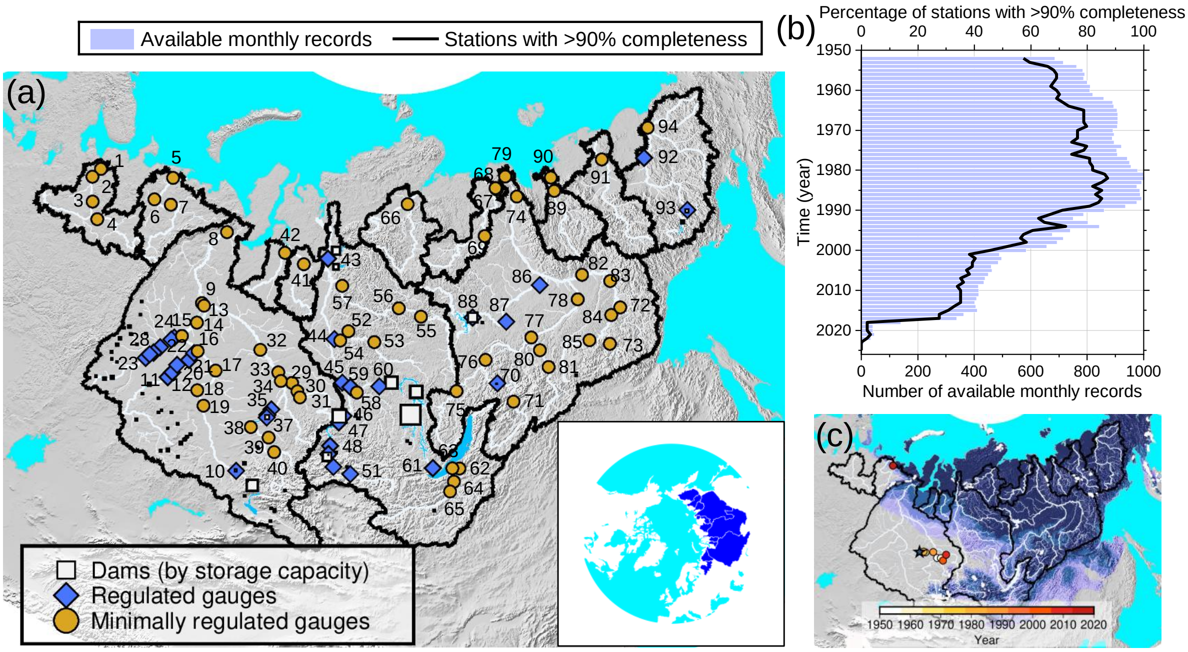

Figure 1. Spatial distribution and temporal availability of river discharge observations in the Eurasian Arctic. (a) Locations of the 94 gauging stations and major dams used in this study. Square size represents reservoir storage capacity, while diamonds and circles denote regulated and minimally regulated gauges, respectively. Dam information was obtained from Lehner et al. (2024) . (b) Annual number of available monthly discharge records among the 94 gauges since 1950 (bars) and the percentage of gauges with annual record completeness exceeding 90% (black line). Data availability was determined from records publicly released by the Global Runoff Data Centre as of 27 February 2026. (c) Temporal migration of the spatial centroid of gauges with available discharge records. After 2010, the centroid shifted toward the downstream reaches of major Eurasian Arctic rivers, reflecting the progressive loss of inland observations. Blue shading indicates permafrost distribution, and white dots indicate glacier distribution.

Hydrological models provide spatially complete and temporally continuous discharge estimates, complementing gauge observations. However, model estimates are sensitive to forcing data, process representation, and parameterization (Lin et al., 2019). Hydrological models differ markedly in interannual variability and seasonal dynamics (Tiwari et al., 2025; Yi et al., 2023). Some models even produce long-term trends with opposite signs in the same region (Hirschi et al., 2025). A recent observation-constrained analysis further indicated that Earth system models overestimate both past and projected increases in global river flow (Zhang et al., 2026).

Advances in satellite remote sensing have enabled the remote monitoring and estimation of river discharge using satellite altimetry, optical imagery, and related techniques (Bjerklie et al., 2018; Feng et al., 2026; Gleason and Smith, 2014; Scherer et al., 2024; Zakharova et al., 2020). The recently launched Surface Water and Ocean Topography mission jointly observes river water levels, widths, and surface slopes, providing new capabilities for global discharge estimation (Andreadis et al., 2025; Vinogradova et al., 2025). However, conventional satellite observations are constrained by revisit intervals, spatial sampling, and minimum observable

https://doi.org/10.5194/essd-2026-531
Preprint. Discussion started: 10 August 2026

channel widths, limiting their ability to provide spatially and temporally continuous long-term discharge records, particularly for Arctic rivers (Bjerklie et al., 2018; Coss et al., 2020).

Since 2002, the Gravity Recovery and Climate Experiment (GRACE) and its successor mission, GRACE Follow-On (GRACE-FO), have provided observations of TWS variations (Rodell and Reager, 2023; Tapley et al., 2019), offering an additional approach for runoff estimation. One approach derives discharge from precipitation, evapotranspiration, and TWS changes using the water balance equation (Chen et al., 2020; Sneeuw et al., 2014). However, its estimates are sensitive to errors in the hydroclimatic inputs and to noise amplified by the temporal differentiation of GRACE TWS. An alternative uses an empirical runoff–TWS relationship to estimate river discharge (Riegger and Tourian, 2014). Although its spatial applicability is limited, the empirical runoff–TWS relationship generally outperforms the conventional water balance method in regions where it is applicable (Sneeuw et al., 2014). Yi et al. (2023) extended this relationship to high-latitude basins by accounting for snow dynamics, but limitations remain in reproducing interannual variability and extreme events (Leopardi et al., 2026). Moreover, the limited duration of the GRACE TWS records limits river discharge reconstruction prior to the GRACE era.

In recent years, machine learning and empirical approaches for reconstructing historical GRACE-like TWS have developed rapidly. Several reconstructed products can statistically reproduce TWS signals similar to those observed by GRACE (-FO) (Gentner et al., 2026; Hacker et al., 2026; Humphrey and Gudmundsson, 2019; Li et al., 2021; Liu et al., 2021, 2022; Xie and Yi, 2026; Yin et al., 2023), making it possible to recover missing historical discharge information using the empirical runoff–TWS relationship. However, existing TWS reconstruction approaches still have several limitations. Machine learning approaches often lack explicit physical constraints and a unified theoretical framework, and their reconstruction performance may vary substantially among regions. Some empirical models reconstruct only deseasonalized and detrended TWS variations (Humphrey and Gudmundsson, 2019; Xie and Yi, 2026), or have limited regional applicability and cannot be directly applied to the Eurasian Arctic (Liu et al., 2021).

In this study, we present a gauge-based monthly natural discharge reconstruction dataset for 94 gauging stations in the Eurasian Arctic from 1952 to 2025. Natural discharge is defined as the discharge expected in the absence of direct human regulation. The dataset was generated using a basin-scale empirical framework in which TWS serves as the key link connecting precipitation and air temperature inputs to river discharge. Historical TWS was reconstructed using an improved state-update empirical model constrained by GRACE TWS observations, and monthly natural discharge was then estimated from reconstructed TWS using a refined runoff–TWS relationship calibrated against gauge-observed discharge. The improved TWS reconstruction model represents solid TWS as a distinct dynamic component, and the refined runoff–TWS relationship distinguishes discharge responses to liquid TWS between snowmelt and non-snowmelt periods. The dataset was evaluated using multiple validation strategies and compared with existing models and reconstruction products. Example applications are provided to illustrate its use for examining regional-scale discharge trends, changes in seasonal distribution, and the effects of human regulation at major river outlets. This dataset provides a long-term natural-discharge baseline for characterizing historical discharge variability and assessing the roles of climate variability and human regulation in poorly monitored cold regions.

2 Data

2.1 Reference data

GRACE TWS and river discharge records were used as reference data in this study. TWS anomalies derived from GRACE mascon products were used to constrain the historical TWS reconstruction. Three mascon products were obtained from the Center for

https://doi.org/10.5194/essd-2026-531
Preprint. Discussion started: 10 August 2026

Open Access Earth System Science Data Discussions

Space Research (CSR; Save et al., 2016), the Jet Propulsion Laboratory (JPL; Watkins et al., 2015; Wiese et al., 2016), and the Goddard Space Flight Center (GSFC; Loomis et al., 2019; Luthcke et al., 2013). Before calculating basin-total TWS anomaly time series, all three products were resampled to a common 0.5º grid.

Monthly discharge observations from 94 gauging stations in the Eurasian Arctic were obtained from the Global Runoff Data Centre (GRDC) and used as reference data for discharge reconstruction and evaluation. To account for GRACE's effective spatial resolution, only gauges with drainage areas greater than 90,000 km² were selected. Each gauge also contained more than 20 years of available monthly records to ensure sufficient temporal coverage for subsequent evaluation.

2.2 Forcing and auxiliary data

The forcing data included precipitation and air temperature. The reliability of meteorological datasets in the Eurasian Arctic remains uncertain because of sparse station coverage and limited sampling (Lauer et al., 2023). We therefore used multiple precipitation and temperature products to reduce dependence on any single dataset and to characterize uncertainty in the forcing data. The auxiliary data included snow water equivalent (SWE) and snow cover datasets.

Eight combinations of precipitation and temperature datasets (Table 1), together with five SWE products (Table 2), were used to reconstruct historical TWS variations for the contributing area of each gauge. The SWE products were used to estimate changes in basin-scale snow storage. To ensure consistency, all gridded datasets were resampled onto a common 0.5º grid and converted to monthly resolution.

The five SWE products and two snow cover datasets (Table 3) were further used as auxiliary inputs to convert the reconstructed historical TWS into river discharge time series.

This study required separating precipitation into solid and liquid components. JRA-3Q, ERA5 single, and GLDAS NOAH datasets provided explicit rainfall and snowfall fields. For the remaining datasets, precipitation was partitioned using a gridded 50% rain–snow air temperature threshold for the Northern Hemisphere following Jennings et al. (2018).

Table 1. Gridded precipitation and temperature combinations used in this study. P represents precipitation, and T represents air temperature.

Combination	Production	Version	Type	Spatial resolution	Resample	Time resolution	Time coverage	Reference
CRU	CRU	ts 4.09	P & T	0.50°	/	Monthly	1901–2024	Harris et al. (2020)
GPCC	GPCC	v2025	P	0.50°	/	Monthly	1891-2024	Schirmeister et al. (2025)
	BEST	/	T	1.00°	0.50°	Monthly	1850-2024	Rohde & Hausfather, (2020)
U. Delaware	U. Delaware	5.01	P & T	0.50°	/	Monthly	1900–2017	Willmott & Matsuura, (1995)
WaterGAP 20crv3-w5e5	WaterGAP 20crv3-w5e5	2.2e	P	0.50°	/	Monthly	1901–2019	Müller Schmied et al. (2024)
	BEST	/	T	1.00°	0.50°	Monthly	1850−2024	Rohde & Hausfather, (2020)
CPC	CPC	/	P & T	0.50°	/	Daily	1979–2025	Xie et al. (2007); M. Chen et al. (2008)
JRA-3Q	JRA-3Q		P & T	0.25°	0.50°	Monthly	1947-2025	Kosaka et al. (2024)
ERA5 single	ERA5 single	/	P & T	0.25°	0.50°	Monthly	1940–2025	Hersbach et al. (2020)
GLDAS NOAH	GLDAS NOAH	020	P & T	0.25°	0.50°	Monthly	1948–2014	Rodell et al. (2004)

Table 2. Gridded Snow Water Equivalent (SWE) datasets used in this study.

https://doi.org/10.5194/essd-2026-531
Preprint. Discussion started: 10 August 2026

Name	Version	Spatial resolution	Resample	Time resolution	Time coverage	Reference
ERA5-land		0.10°	0.50°	Monthly	1950−2025	Muñoz-Sabater et al. (2021)
Crocus-ERA5		0.25°	0.50°	Monthly	1950–2023	Ramos Buarque et al. (2025)
WaterGAP 20crv3-w5e5	2.2e	0.50°	/	Monthly	1901–2019	Müller Schmied et al. (2024)
GLDAS NOAH	020	0.25°	0.50°	Monthly	1948–2014	Rodell et al. (2004)
JAR-3Q		0.25°	0.50°	Monthly	1947-2025	Kosaka et al. (2024)

Table 3. Gridded snow cover datasets used in this study.

Name	Spatial resolution	Resample	Time resolution	Time coverage	Reference
ERA5-land	0.10°	0.50°	Monthly	1950−2020	Muñoz-Sabater et al. (2021)
Crocus-ERA5	0.25°	0.50°	Monthly	1950–2023	Ramos Buarque et al. (2025)

3 Methods

3.1 Improved empirical model for TWS reconstruction in the Eurasian Arctic

Basin-scale TWS observations from GRACE are available only since 2002. Because reconstructing river discharge before 2002 requires historical TWS information, earlier TWS variations must first be estimated. Liu et al. (2021) developed a state-update empirical model that estimates current TWS from precipitation, air temperature, and the preceding TWS state (Text S1). However, the model does not represent the asynchronous responses of solid TWS (TWS^{solid}) accumulation and melt relative to liquid TWS (TWS^{liquid}), limiting its applicability to rainfall-driven liquid water processes and reducing its suitability for cold basins in the Eurasian Arctic.

To extend the model to the Eurasian Arctic, precipitation and TWS were separated into solid and liquid components. Because melt induced liquid TWS dynamics cannot be represented by concurrent precipitation alone, an additional meltwater term, $\Delta TWS^{\text{solid}}$, was introduced during the melt period. This term represents the contribution of declining solid water storage to liquid TWS dynamics and was derived from month-to-month changes in solid TWS. The term α_w represents the fraction of solid precipitation (P^{solid}) that directly contributes to liquid hydrological processes, with ranges from 0 to 1. Given the limited glacier coverage within the study region (Figure 1c), solid TWS was approximated by snow storage.

$$TWS^{\text{liquid}}_{t_{i+1}} + d_w = \left(TWS^{\text{liquid}}_{t_i} + d_w\right) \cdot e^{\tau^*_{t_{i+1}}} + P^{\text{liquid}}_{t_{i+1}} + \alpha_w \cdot P^{\text{solid}}_{t_{i+1}} + \Delta TWS^{\text{solid}}_{t_{i+1}} \tag{1}$$

$$\Delta TWS^{\text{solid}}_{t_i} = \max\left(TWS^{\text{solid}}_{t_{i-1}} - TWS^{\text{solid}}_{t_i}, 0\right) \tag{2}$$

$$TWS^{\text{liquid}}_{t_i} = TWS_{t_i} - TWS^{\text{solid}}_{t_i} \tag{3}$$

The residual function (τ^*) was revised in four respects. First, precipitation was removed from the residual function because precipitation and temperature exhibit similar seasonal cycles in the Eurasian Arctic and may introduce multicollinearity when used together. Second, temperature was partitioned at 0 °C into temperature above freezing (T^{melt}) and below freezing (T^{freeze}). The latter was used to simulate the potential effects of baseflow and sublimation during freezing periods. Third, meltwater term ($\Delta TWS^{\text{solid}}$) was included during melt periods to represent their additional influence on residual TWS. Finally, a lag parameter

https://doi.org/10.5194/essd-2026-531
Preprint. Discussion started: 10 August 2026

(ω), with ranges from 0 to 1, was introduced to potentially delayed hydrological process. $*'$ indicates the normalized form of these variables. The improved model contained seven parameters, (a, b_1, b_2, c, d_w, α_w, and ω), which were estimated using GRACE TWS anomalies as reference observations.

$$\tau^*_{t_{i+1}} = a + b_1 \cdot \left(T^{\text{freeze}}_{t_{i+1}} - \min\left(T^{\text{freeze}}\right)\right)' + b_2 \cdot \omega \cdot T^{\text{melt}'}_{t_i} + b_2 \cdot (1-\omega) \cdot T^{\text{melt}'}_{t_{i+1}} + c \cdot \Delta TWS^{\text{solid}'}_{t_{i+1}} \quad (4)$$

3.2 Refined Runoff-TWS Relationship

Yi et al. (2023) extended the runoff–TWS relationship of Riegger and Tourian (2014) to the pan-Arctic by separating the solid TWS that does not directly contribute to runoff generation (Text S2). The method assumes that runoff (R) is proportional to liquid TWS (TWS^{liquid}) at adjacent monthly time steps, while snow cover fraction (SC) modulates this relationship under different hydraulic connectivity conditions.

However, Yi et al. (2023) used constant hydraulic coefficients α_1 and α_2 to describe the runoff response to liquid TWS. Because the runoff response of surface meltwater may differ from that of background liquid storage, these constant coefficients may represent an averaged response across contrasting hydrological regimes, leading to underestimated runoff during snowmelt periods and overestimated runoff during non-snowmelt periods.

Accordingly, we further refined the model of Yi et al. (2023) by introducing two additional perturbation coefficients, μ_1 and μ_2, to adjust the hydraulic coefficients according to meltwater intensity. This formulation allows the effective hydraulic coefficients to differ between snowmelt and non-snowmelt periods. Meltwater intensity was represented by the normalized meltwater term ($\Delta TWS^{\text{solid}'}$). Consistent with the TWS reconstruction model, solid TWS was approximated by snow storage.

$$R_{t_{i+1}} = \left(\alpha_1 + \mu_1 \cdot \Delta TWS^{\text{solid}'}_{t_i}\right) \cdot \left(1 - \beta \cdot SC_{t_i}\right) \cdot \left(TWS^{\text{liquid}}_{t_i} + d_r\right) + \left(\alpha_2 + \mu_2 \cdot \Delta TWS^{\text{solid}'}_{t_{i+1}}\right) \cdot \left(1 - \beta \cdot SC_{t_{i+1}}\right) \cdot \left(TWS^{\text{liquid}}_{t_{i+1}} + d_r\right) \quad (5)$$

Equations (1) and (5) include the storage-offset parameters d_w and d_r, respectively, to offset the unknown storage baseline because GRACE provides TWS anomalies rather than absolute storage. Their values may differ within the same contributing area because they are estimated in different model structures and from different inputs. Specifically, d_w may vary with the selected precipitation and SWE products, whereas d_r mainly depends on the SWE product.

In the method of Yi et al. (2023), GRACE TWS is detrended before runoff estimation to reduce the influence of mass loss from glaciers and permafrost, as well as residual geophysical signals. Because these non-target signals are not included in our reconstructed TWS, no detrending was applied before runoff estimation.

3.3 Ensemble Reconstruction and Uncertainty Estimation

A fixed-SWE ensemble strategy was used to reconstruct natural discharge. For each SWE product and contributing area, eight precipitation and temperature combinations were paired with three GRACE mascon products, producing 24 historical TWS reconstructions. Their ensemble mean was taken as the TWS reconstruction corresponding to that SWE product. This TWS series was then combined with two snow cover products to generate two natural discharge reconstructions. Because five SWE products were used, each gauge yielded a 10-member natural discharge ensemble. The ensemble mean was adopted as the final monthly natural discharge reconstruction for January 1952 to December 2025. The reconstruction process is shown in Figure 2.

Model parameters were estimated using a Markov chain Monte Carlo (MCMC) algorithm. Parameters of the TWS reconstruction model were identified over 2003–2012, whereas the discharge reconstruction parameters were identified over a gauge-specific 10-

https://doi.org/10.5194/essd-2026-531
Preprint. Discussion started: 10 August 2026

year period selected according to discharge data availability (Figure 3a). For gauges strongly affected by human regulation, this 10-year period was restricted to the pre-regulation period.

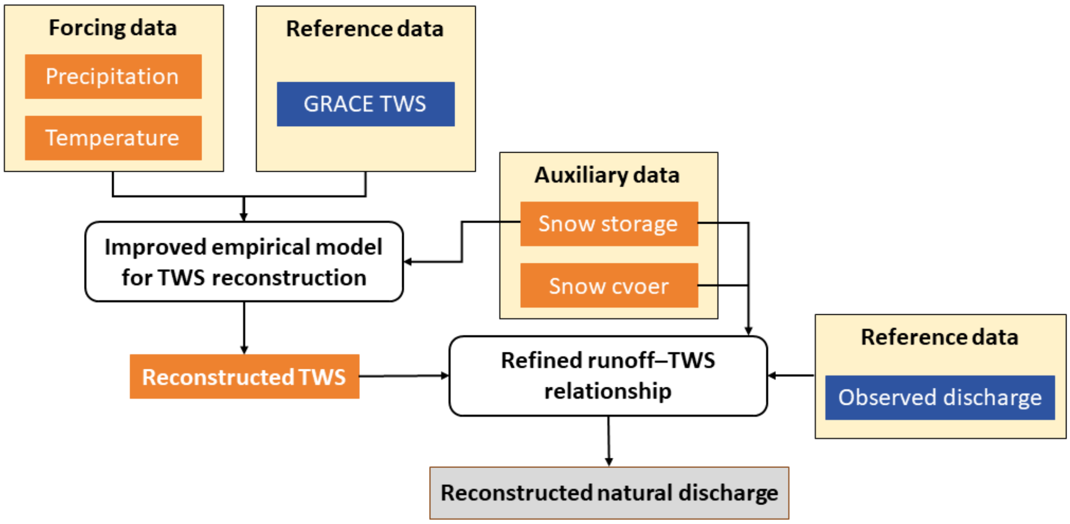

Figure 2. Flowchart of the monthly natural discharge reconstruction framework in this study.

The uncertainty in the reconstructed natural discharge included parameter uncertainty (σ_p) and forcing-data uncertainty (σ_f). Parameter uncertainty was defined as one standard deviation among the reconstructions generated from 20,000 accepted MCMC samples. Forcing-data uncertainty was defined as one standard deviation of the 10-member discharge ensemble. The total uncertainty was calculated as the root-sum-square of parameter and forcing-data uncertainties.

$$\sigma_{\mathrm{runoff_{Recon}}} = \sqrt{\left(\sum_{s=1}^{N} \sigma_p^2 / N^2\right) + \sigma_f^2} \tag{6}$$

4 Evaluation

4.1 Monthly discharge evaluation

Based on the distribution of major dams in the Eurasian Arctic, the 94 gauges were broadly classified into 61 minimally regulated gauges (Figure 1a, circles) and 33 regulated gauges (Figure 1a, diamonds).

For the 61 minimally regulated gauges, training and testing experiments were conducted to evaluate the framework's ability to simulate and extrapolate natural discharge. The training period corresponded to the parameter identification period (Figure 3a, gray shading), and the remaining observations were used for testing. For the 33 regulated gauges, the evaluation was divided into pre-regulation and post-regulation periods. The pre-regulation period was used to further assess the reliability of the reconstructed monthly natural discharge, whereas the post-regulation period (Figure 3a, light-blue shading) was used to examine the effects of human regulation on discharge.

At the minimally regulated gauges, reconstructed natural discharge agreed well with observations during both the training and testing periods (Figure 3b). The median monthly Kling–Gupta efficiency (KGE) values were 0.92 and 0.88 for the training and testing periods, with standard deviations of 0.04 and 0.08, respectively. These results demonstrate that the framework can simulate monthly natural discharge during parameter identification and extrapolate it to independent periods.

https://doi.org/10.5194/essd-2026-531
Preprint. Discussion started: 10 August 2026

At the regulated gauges, reconstructed and observed discharge agreed well before regulation, with a median monthly KGE of 0.89 and a standard deviation of 0.14 (Figure 3c). After regulation, KGE values decreased at most gauges, indicating reduced agreement between observed discharge and the reconstructed natural discharge. These declines were mainly observed at gauges near dams along the Ob River in the Ob basin, the Yenisei and Angara rivers in the Yenisei basin, and the Vilyuy River in the Lena basin (Figure 3d). In contrast, several gauges along the Tobol River in the Ob basin showed higher post-regulation KGE values, possibly because the dams upstream were relatively small and had limited effects on observed discharge.

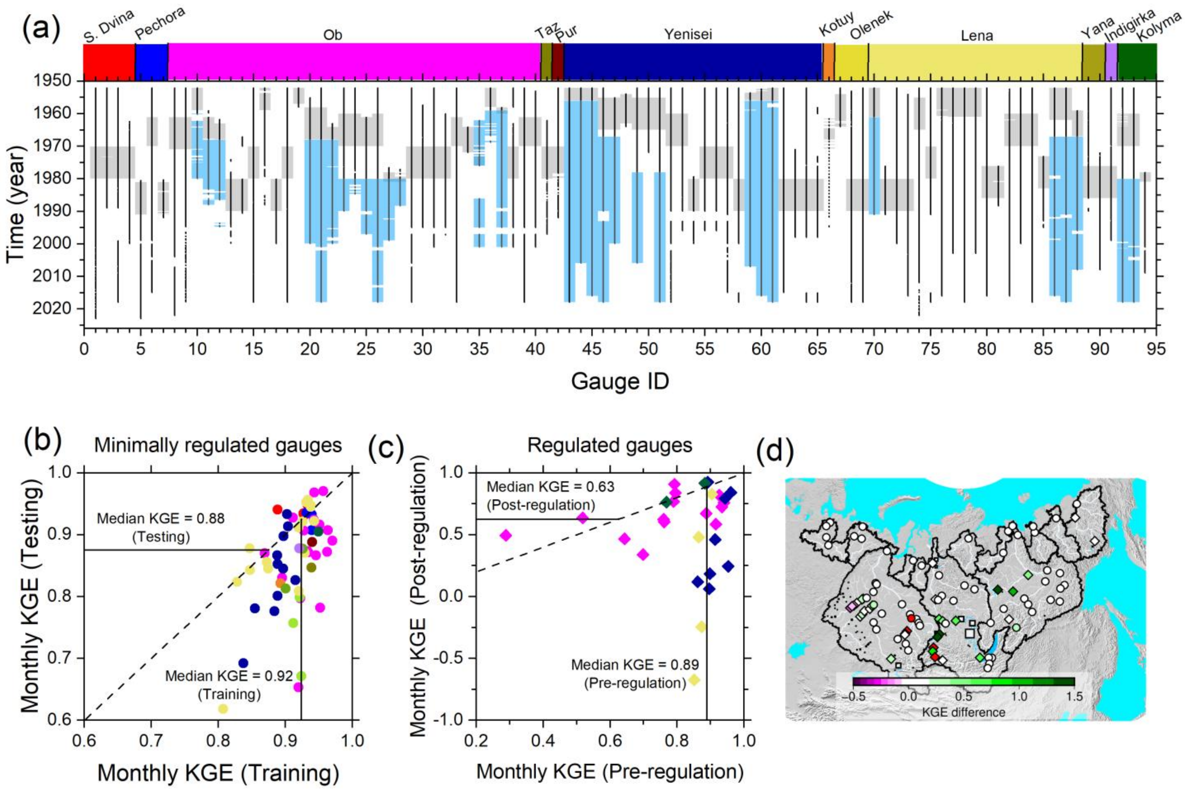

Figure 3. Evaluation of reconstructed monthly natural discharge at 94 gauges in the Eurasian Arctic from January 1952 to December 2025. (a) Availability of observed monthly discharge records. Black lines indicate available observations, gray shading indicates the training and parameter identification period, and light blue shading indicates the post-regulation period. (b) Monthly Kling–Gupta efficiency (KGE) values during the training and testing periods at 61 minimally regulated gauges, with all observations outside the training period used for testing. (c) Monthly KGE values pre- and post-regulation at 33 regulated gauges. Regulation began in the earliest initial impoundment year among upstream dams. (d) Spatial distribution of KGE differences, calculated as testing minus training for minimally regulated gauges and pre-regulation minus post-regulation for regulated gauges.

Many large reservoirs in the Eurasian Arctic are associated with hydropower development, and their operation can redistribute discharge seasonally. After regulation, observed discharge was generally lower than reconstructed natural discharge in summer but higher in winter (Figure 4a), consistent with water storage during the high-flow season and releases during the low-flow season to sustain hydropower generation. The shift in mean seasonal discharge anomalies, calculated as observed minus reconstructed discharge, between the pre- and post-regulation periods further demonstrates this redistribution (Figure 4b).

In contrast, the mean seasonal cycles of reconstructed and observed discharge remained consistent at the minimally regulated gauges throughout the available observation periods (Figure 4c). The means and medians of the mean seasonal discharge anomalies for all 61 gauges were close to zero, further supporting the reliability of the reconstructed natural discharge (Figure 4d).

https://doi.org/10.5194/essd-2026-531
Preprint. Discussion started: 10 August 2026

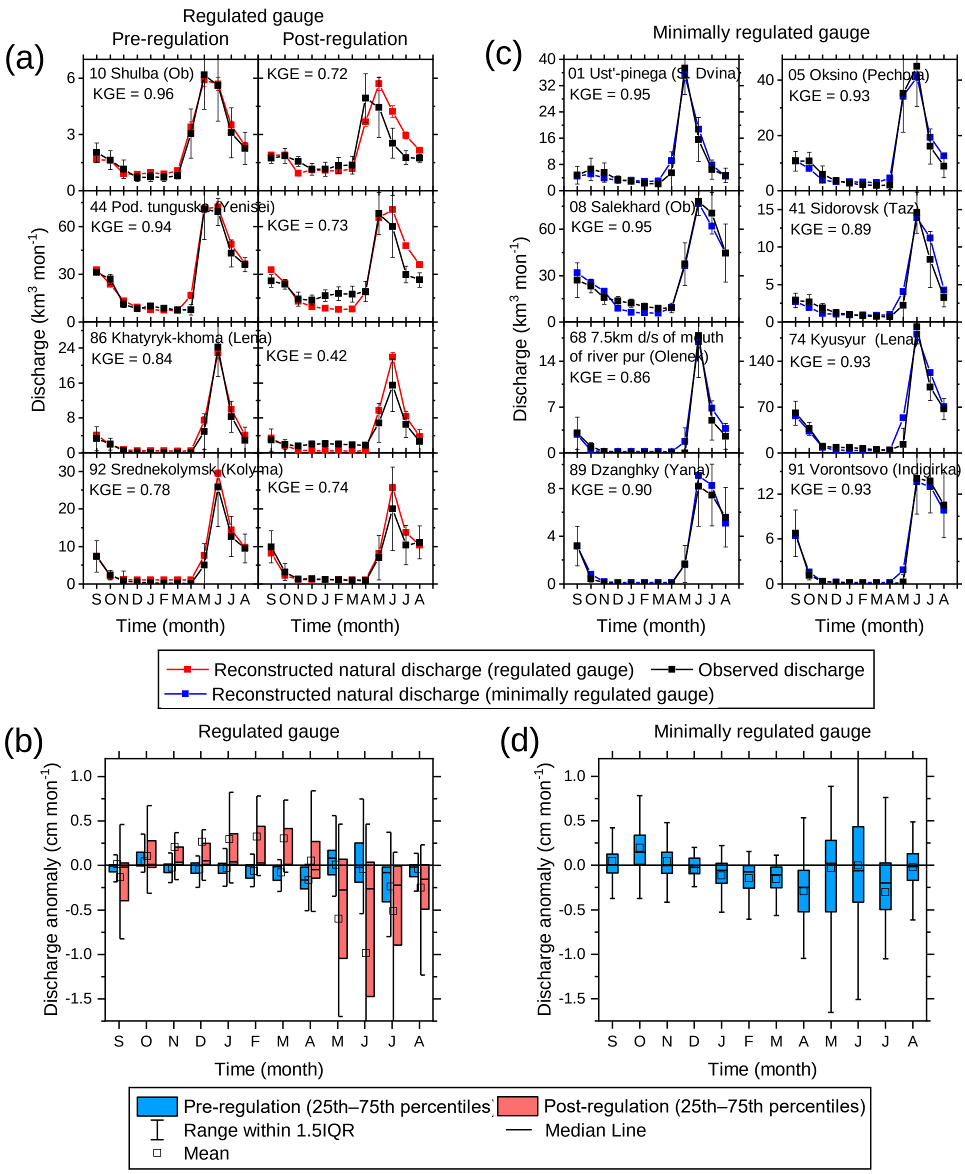

Figure 4. Comparison of mean seasonal discharge cycles between reconstructed natural discharge and observations. (a) Mean seasonal cycles at selected regulated gauges before and after regulation. (b) Mean seasonal discharge anomalies at 33 regulated gauges during the pre-regulation and post-regulation periods, calculated as observed minus reconstructed natural discharge. (c) Mean seasonal cycles at selected minimally regulated gauges. (d) Mean seasonal discharge anomalies at 61 minimally regulated gauges. Boxes indicate the interquartile range, whiskers extend to 1.5 times the interquartile range, and horizontal lines and squares denote the median and mean, respectively.

4.2 Annual discharge and apportionment entropy evaluation

The reconstructed monthly natural discharge was further summed by hydrological year, defined from September to the following August, and compared with observations (Figure 5 and Figure S1). This annual-scale evaluation provides an additional test of the dataset's ability to represent interannual discharge variability. Overall, reconstructed annual natural discharge agreed well with observations at minimally regulated gauges (Figure 5a, b). At the 61 minimally regulated gauges, the median annual KGE was

https://doi.org/10.5194/essd-2026-531
Preprint. Discussion started: 10 August 2026

Open Access Earth System Science Data Discussions

0.73, with a standard deviation of 0.12 (Figure 5c), indicating stable performance among gauges and a good representation of interannual variability. A notable discrepancy occurred at gauge 68 during the 1990s (Figure 5a), mainly because the reconstruction did not reproduce the observed June peak (Figure S2). Because this gauge is located in a region with high thermokarst lake coverage (Jones et al., 2022), additional local hydrological processes may have contributed to the discrepancy, but their role cannot be confirmed from the available data.

Annual KGE values were more variable among the 33 regulated gauges, with a median of 0.52 and a standard deviation of 0.20 (Figure 5c). Lower values were mainly found downstream of major reservoirs in the Ob, Yenisei, and Lena basins. For example, at the Igarka gauge near the outlet of the Yenisei River, observed annual discharge was notably lower than reconstructed natural discharge during the 1960s and 1970s (Figure 5a). This period that broadly coincided with the initial filling of major upstream reservoirs.

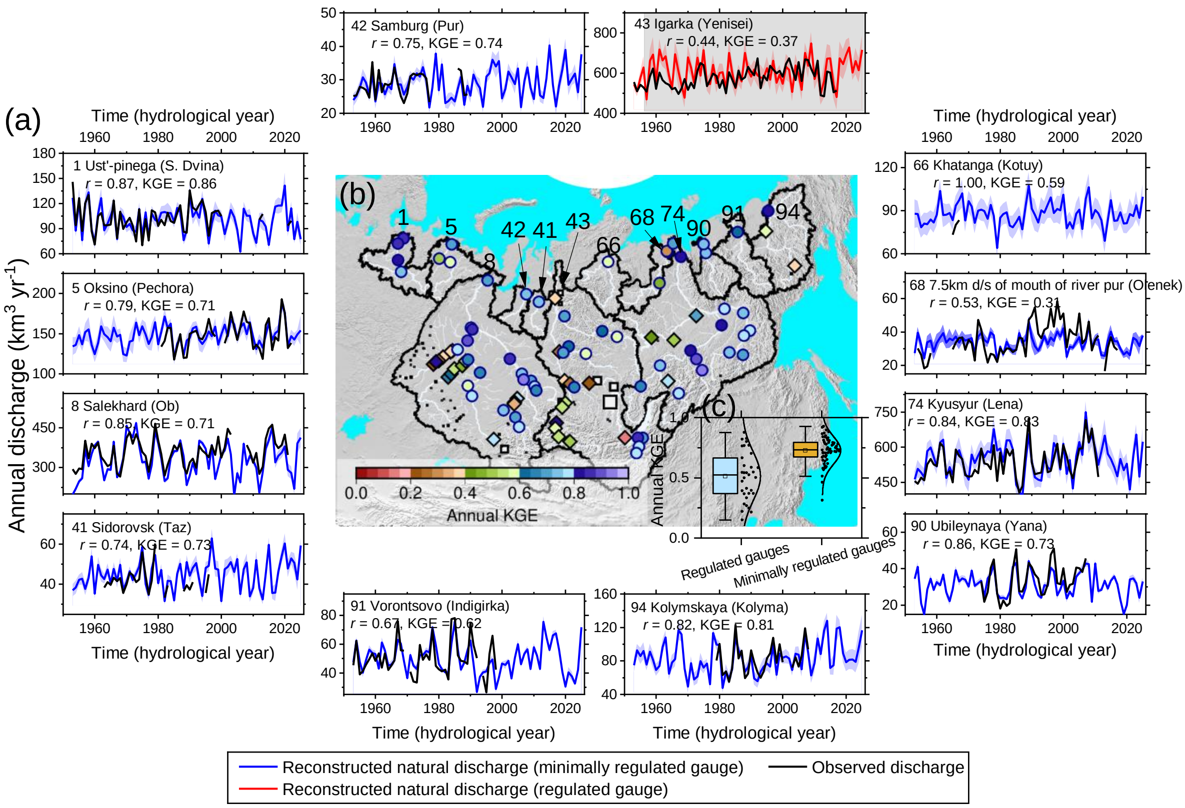

Figure 5. Evaluation of reconstructed annual natural discharge. (a) Time series of reconstructed natural and observed annual discharge at selected gauges. Annual values were aggregated by hydrological year from September to the following August. Shaded interval indicates post-regulation periods. (b) Spatial distribution of annual Kling–Gupta efficiency (KGE) values between reconstructed and observed discharge. (c) Boxplots of annual KGE values at 33 regulated and 61 minimally regulated gauges. More annual runoff time series can be found in Figure S1.

Apportionment Entropy (AE) was further used to evaluate the representation of seasonal discharge allocation. AE is a nonparametric information-theoretic metric derived from Shannon entropy and calculated from monthly discharge fractions, which represent the relative contributions of each month to annual discharge (Feng et al., 2013; Konapala et al., 2020; Wang et al., 2024; Text S3). Higher AE indicates a more even distribution among months, whereas lower AE indicates stronger seasonal concentration.

https://doi.org/10.5194/essd-2026-531
Preprint. Discussion started: 10 August 2026

Open Access Earth System Science Data Discussions

Unlike annual discharge, AE evaluates whether the reconstruction captures year-to-year changes in the within-year allocation of discharge among months.

The reconstructed natural discharge generally reproduced the year-by-year changes in observed discharge seasonality (Figure 6a, b, and Figure S3). At minimally regulated gauges, the median KGE between reconstructed and observed AE was 0.49, with a standard deviation of 0.26 (Figure 6c). At regulated gauges, the median AE KGE decreased to 0.13, with a standard deviation of 0.28, indicating substantial regulation-induced changes in seasonal discharge allocation. At Igarka, observed AE was notably higher than reconstructed natural AE during the post-regulation period (Figure 6a), indicating that upstream reservoir regulation in the Yenisei basin was associated with a more even seasonal distribution of downstream discharge, even near the river outlet.

Larger AE differences at minimally regulated gauges were mainly found at high-latitude gauges in the eastern Eurasian Arctic. At some gauges, such as gauges 68 and 91, reconstructed and observed AE also showed systematic offsets. These differences were largely associated with systematic discrepancies between reconstructed and observed winter low-flow discharge (Figure S4). They may reflect the combined effects of uncertainties in snow-process representation, observational records, and model structure, which can be amplified in AE because this metric is sensitive to the monthly allocation of discharge within a year.

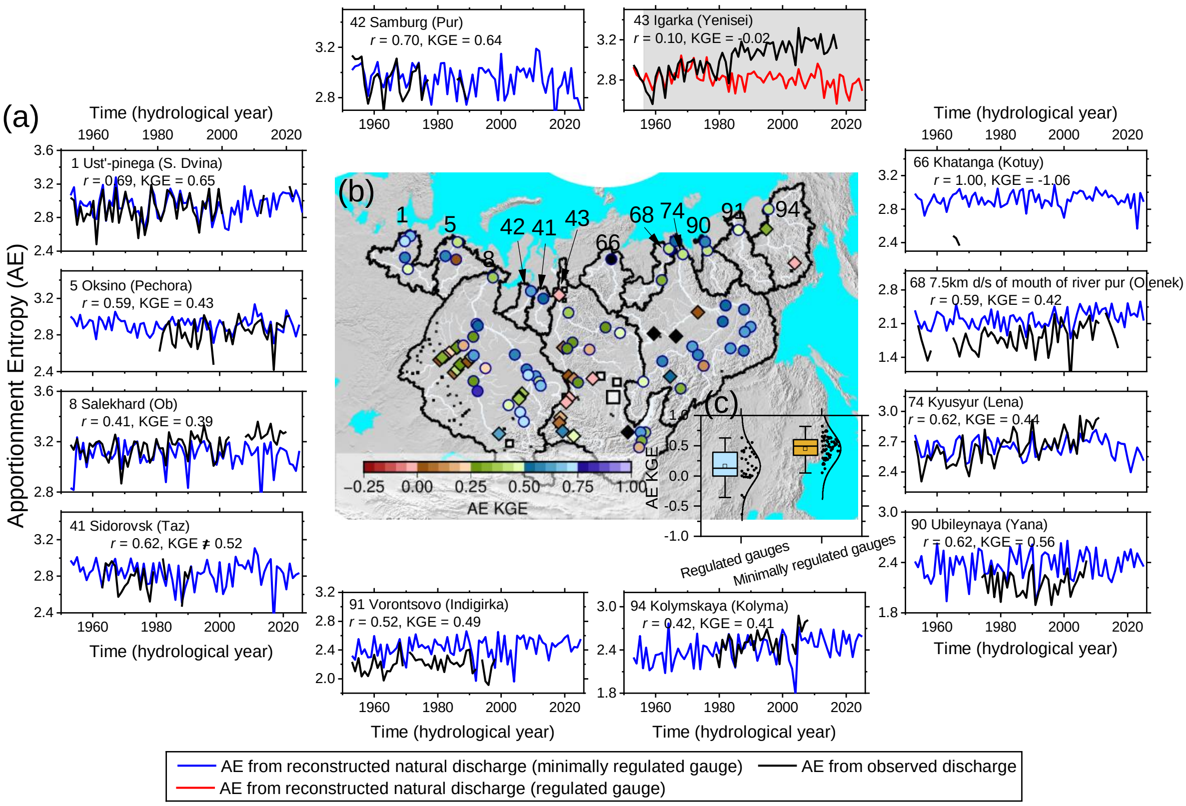

Figure 6. Evaluation of seasonal discharge allocation using Apportionment Entropy (AE). (a) AE time series derived from reconstructed monthly natural discharge and observations at selected gauges. (b) Spatial distribution of Kling–Gupta efficiency (KGE) values between reconstructed and observed AE. (c) Boxplots of AE KGE values at 33 regulated and 61 minimally regulated gauges. More station results can be found in Figure S3.

https://doi.org/10.5194/essd-2026-531
Preprint. Discussion started: 10 August 2026

5 Discussion

5.1 Comparison with discharge estimates from existing GRACE-like TWS products

Historical TWS information is a key input for extending discharge reconstruction before the GRACE era. We therefore examined whether existing publicly available GRACE-like TWS reconstruction products can support comparable gauge-scale discharge estimation in the Eurasian Arctic. Five additional GRACE-like TWS reconstruction products were collected and used to estimate discharge at the 61 minimally regulated gauges. These products include four machine-learning-based reconstructions (Gentner et al., 2026; Hacker et al., 2026; Li et al., 2021; Yin et al., 2023) and one statistical model reconstruction (Humphrey and Gudmundsson, 2019). Unlike the other machine-learning-based products, the reconstruction of Hacker et al. (2026) uses not only climatic predictors but also low-resolution geodetic TWS constraints derived from observations such as satellite laser ranging. In addition, Humphrey and Gudmundsson (2019) did not reconstruct the seasonal TWS component directly; the seasonal signal in their product was estimated from GRACE TWS observations.

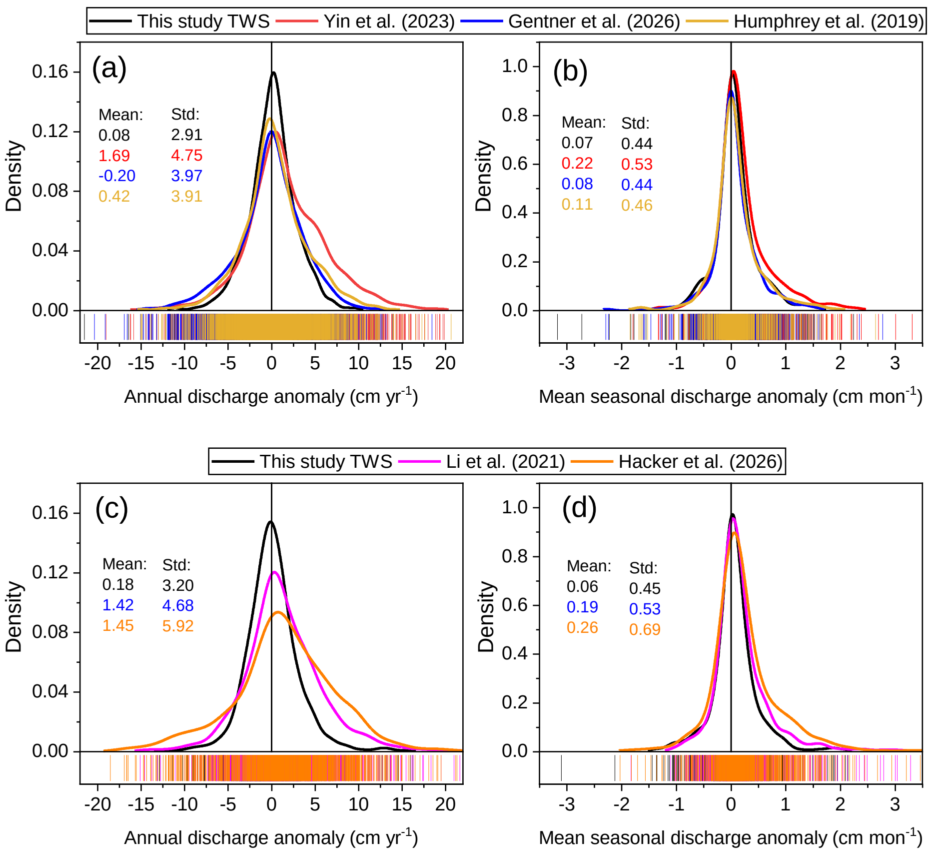

Figure 7. Comparison of discharge estimates derived from different TWS reconstruction products with observed discharge at 61 minimally regulated gauges. Discharge anomalies were calculated as observed minus reconstructed discharge and normalized by each gauge's contributing area. (a, b) Comparisons between the TWS reconstruction developed in this study and three products extending to the pre-1950 period: Yin et al. (2023), Gentner et al. (2026), and Humphrey and Gudmundsson (2019). The evaluation period was fixed to 1953–2018 for consistency. (a) Distribution of annual discharge anomalies. (b) Distribution of mean seasonal discharge anomalies. (c, d) Comparisons between the TWS reconstruction developed in this study and two products available only after the 1980s: Li et al. (2021) and Hacker et al. (2026). For consistency, the parameter identification period for discharge reconstruction was restricted to the period after 1985, and the evaluation period was fixed to 1985–2020. (c) Distribution of annual discharge anomalies. (d) Distribution of mean seasonal discharge anomalies. Rug marks indicate individual gauge values.

Discharge estimates based on the TWS reconstruction developed in this study showed anomaly distributions (observation minus reconstruction) that were more concentrated around zero than those based on the other GRACE-like TWS products. This difference was most evident for annual discharge anomalies. For the 1953–2018 comparison (Figure 7a), this study had an annual discharge anomaly with a mean of 0.08 cm yr^{-1} and a standard deviation of 2.91 cm yr^{-1}. Its absolute mean anomaly and spread were smaller than those obtained from Yin et al. (2023), Gentner et al. (2026), and Humphrey and Gudmundsson (2019). For the 1985–2020 comparison (Figure 7c), this study also showed a smaller absolute mean anomaly and narrower spread than those derived Li et al. (2021) and Hacker et al. (2026). These results indicate that, within the discharge reconstruction framework used here, the TWS reconstruction developed in this study led to smaller bias and lower error dispersion in annual discharge estimation for the Eurasian Arctic.

Differences among products were smaller for the mean seasonal cycle (Figure 7b and d). Seasonal discharge anomalies from all products were generally centered near zero, suggesting that existing GRACE-like TWS reconstructions retain much of the seasonal information needed for discharge estimation. However, anomaly distributions from this study were still slightly narrower, particularly compared with products available only after the 1980s (Figure 7d). Overall, within the Eurasian Arctic and under the discharge reconstruction framework used here, the TWS reconstruction developed in this study produced discharge estimates with smaller errors than those based on the examined GRACE-like TWS products, particularly at the annual scale. These results suggest that existing GRACE-like TWS reconstructions can provide useful seasonal information in this region, but their ability to support interannual gauge-scale discharge reconstruction remains more uncertain.

5.2 Comparison with an existing gridded discharge reconstruction product

We further compared the reconstructed gauge-based natural discharge with GRUN, an existing 0.5° gridded runoff reconstruction product (Ghiggi et al., 2019). GRUN reconstructs monthly runoff using machine learning, with precipitation and air temperature as predictors and in situ discharge observations as constraints. Because GRUN does not explicitly account for human regulation of river discharge, it provides a useful reference dataset for comparison with the reconstructed natural discharge developed in this study.

Because GRUN is a gridded runoff product, discharge estimates aggregated from GRUN over gauge contributing areas are not strictly equivalent to observed discharge at gauge outlets. Differences may arise from spatial aggregation, basin-boundary discretization, runoff routing, and seasonal phase shifts. We therefore focused on variability rather than absolute magnitude. Observed and reconstructed discharge were first demeaned over their common reference period, and demeaned discharge residuals were then calculated as observed demeaned discharge minus reconstructed demeaned discharge.

Figure 8 compares the demeaned discharge residuals derived from this study and GRUN at the 61 minimally regulated gauges. For the mean seasonal cycle, large residuals were mainly concentrated during warm-season high-flow months, indicating differences in the representation of snowmelt and summer discharge (Figure 8a). Compared with GRUN, this study produced smaller residuals and lower RMSE at nearly all gauges (Figure 8b), with RMSE reductions exceeding 50% at 51 gauges.

At the annual scale, the demeaned discharge residuals derived from this study and from GRUN showed similar interannual fluctuations, although RMSE values were generally lower for this study (Figure 8c, d). Even at gauge 68, where annual reconstructed discharge differed markedly from observations in Figure 5a, the residuals derived from this study and from GRUN showed similar year-to-year variability, further indicating the consistency between the two reconstructions in representing annual variability.

https://doi.org/10.5194/essd-2026-531
Preprint. Discussion started: 10 August 2026

Overall, these results suggest that the reconstructed records developed here agree more closely with gauge observations than discharge estimates aggregated from GRUN. However, because GRUN is a gridded runoff product, its conversion to gauge-scale discharge may introduce uncertainties. Therefore, this comparison does not demonstrate that the framework in this study is generally superior to GRUN, but indicates that our dataset is more consistent with gauge-scale observations for the Eurasian Arctic gauges examined here.

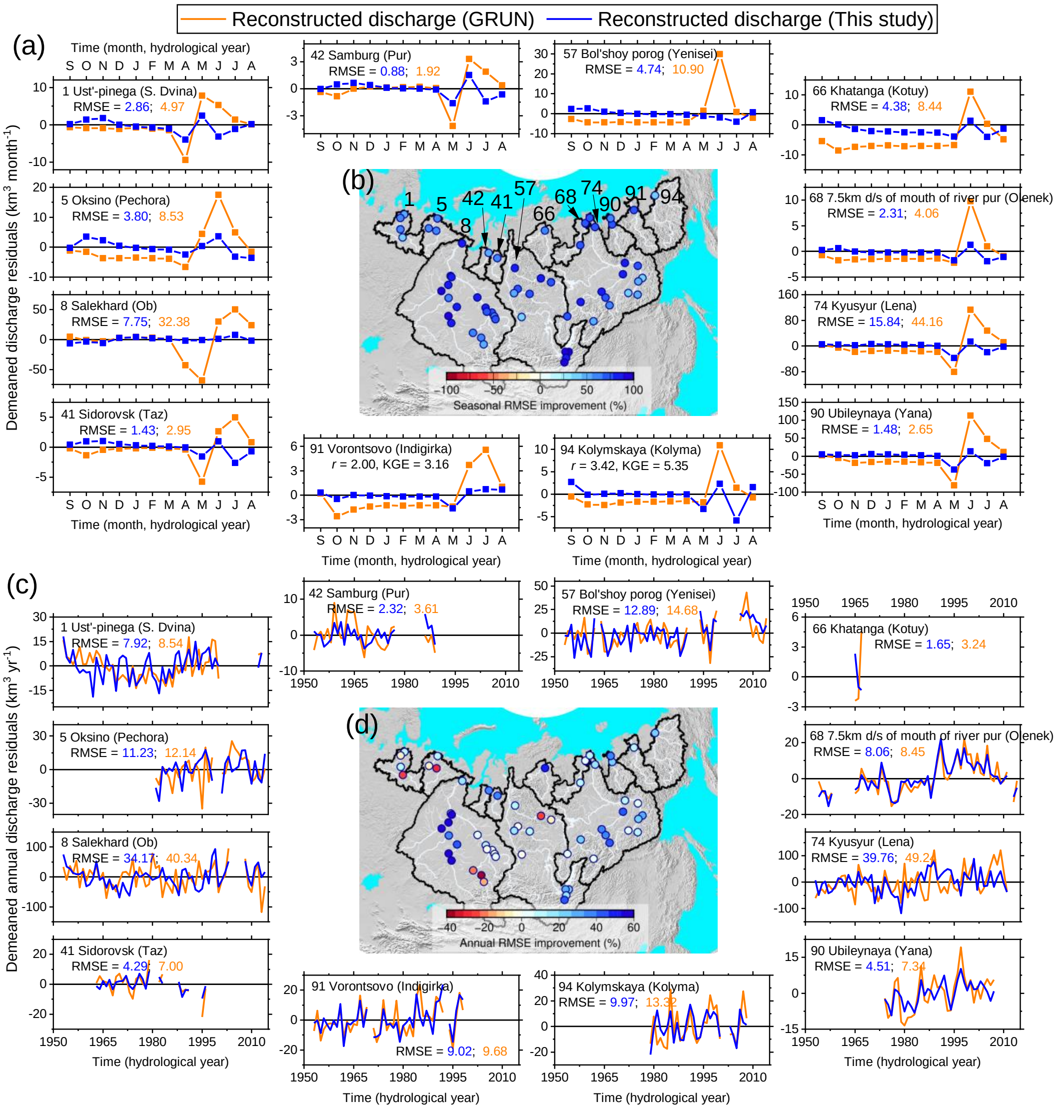

Figure 8. Comparison of demeaned discharge residuals at the mean seasonal and annual scales. Observed and reconstructed discharge were first demeaned over their common reference period. Demeaned discharge residuals were then calculated as observed demeaned discharge minus reconstructed demeaned discharge. (a) Mean seasonal demeaned discharge residuals derived from this study and from GRUN at selected gauges. (b) RMSE improvement of this study relative to GRUN for the mean seasonal cycle at the 61 minimally regulated gauges. (c) Annual demeaned discharge residuals derived from this study and from GRUN at selected gauges. (d) RMSE improvement of this study relative to GRUN for annual discharge at the 61 minimally regulated gauges.

https://doi.org/10.5194/essd-2026-531
Preprint. Discussion started: 10 August 2026

5.3 Comparison with the previous runoff–TWS relationship

We compared the refined runoff–TWS relationship used in this dataset with the previous formulation of Yi et al. (2023) in terms of annual discharge and the mean seasonal cycle. For cross-gauge comparison, discharge at each gauge was normalized by its contributing area. At the 61 minimally regulated gauges, annual discharge anomalies, defined as observed minus reconstructed values, were more concentrated around zero for the refined relationship (Figure 9a). The mean anomaly shifted from −0.23 to −0.08 cm yr^{-1}, while the standard deviation decreased from 3.41 to 2.91 cm yr^{-1}, indicating reduced systematic bias and lower error dispersion among gauges. Annual RMSE decreased at 53 of the 61 gauges (86.9%), with reductions exceeding 30% at 13 gauges and 45% at three gauges (Figure 9b).

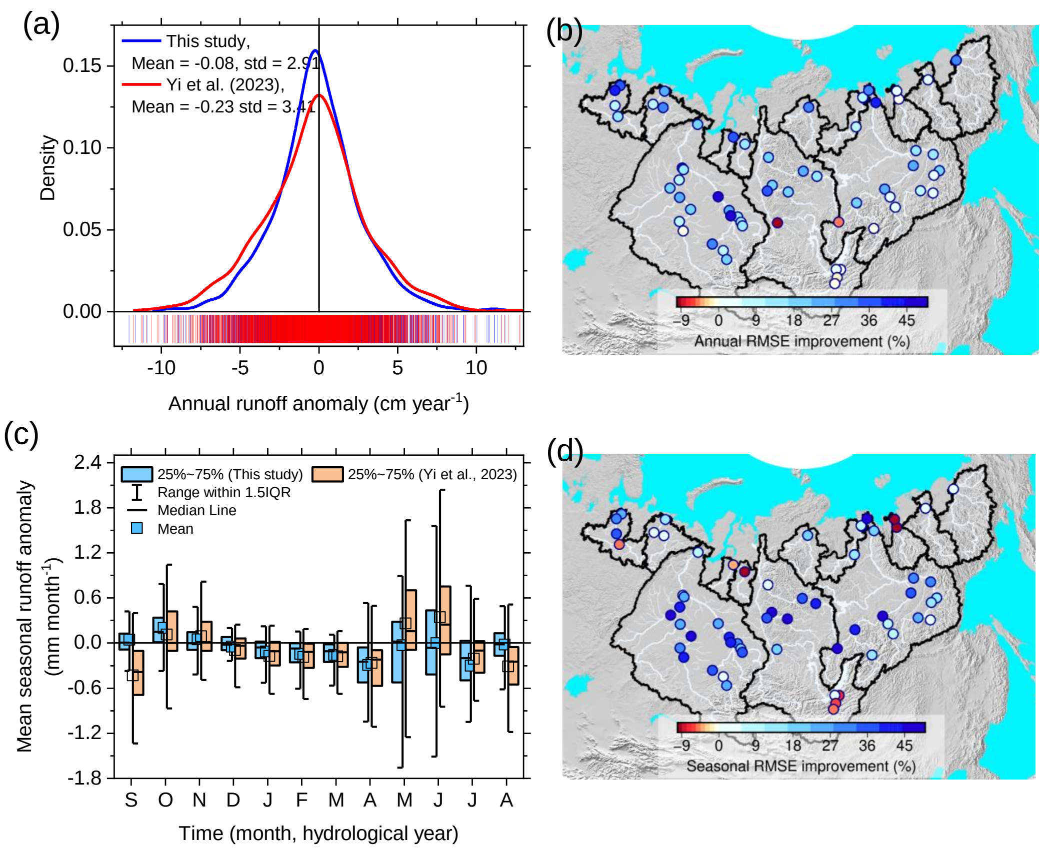

Figure 9. Performance comparison between the refined runoff–TWS relationship developed in this study and the relationship of Yi et al. (2023) at 61 minimally regulated gauges. (a) Probability density distributions of annual discharge anomalies, calculated as observed minus reconstructed values. Rug marks indicate individual gauge values. (b) Spatial distribution of annual root mean square error (RMSE) improvement relative to Yi et al. (2023). (c) Monthly distributions of mean seasonal-cycle anomalies for the hydrological year from September to the following August. Horizontal lines and squares indicate the median and mean, respectively. (d) Spatial distribution of RMSE improvement for the mean seasonal cycle. Positive values indicate lower RMSE for the refined relationship, whereas negative values indicate performance degradation.

The added value of the refined relationship was more evident for the mean seasonal cycle. The means and medians of monthly anomalies from the refined relationship were close to zero in most months (Figure 9c). In contrast, the previous relationship produced predominantly negative anomalies in August and September and from December to March, but positive anomalies in May and June. Because anomalies were calculated as observed minus reconstructed discharge, these patterns suggest that the previous relationship tended to overestimate discharge during predominantly non-snowmelt months and underestimate it during the main snowmelt months. This seasonal bias may arise because the previous relationship uses constant hydraulic coefficients that represent average discharge responses under contrasting snowmelt and non-snowmelt conditions. By adding perturbation terms to the hydraulic coefficients during snowmelt, the refined relationship better distinguishes discharge responses between these two conditions. RMSE for the mean seasonal cycle also decreased at 53 of the 61 gauges (86.9%), with reductions exceeding 30% at 22 gauges and 45% at six gauges (Figure 9d).

Gauge-to-gauge differences in RMSE changes showed no clear longitudinal or latitudinal pattern, and RMSE increased at a small number of gauges. These differences may be related to the relative contribution, timing, and duration of snowmelt, as well as contrasts between melt-driven and rainfall-driven discharge responses. Where snowmelt contributes only a small fraction of annual discharge, distinguishing these responses may provide limited additional benefit. Uncertainties in meteorological forcing, SWE and snow cover products, and observed discharge may also affect the estimated performance changes. Overall, the refined runoff–TWS relationship improved the representation of the mean seasonal cycle at most minimally regulated gauges, supporting its use in the reconstructed monthly natural discharge dataset.

5.4 Dataset limitations

Although the reconstructed dataset provides long-term monthly natural discharge records for the Eurasian Arctic, several limitations should be considered when using the data. First, the reconstruction depends on external information on solid-water storage. For most snow-dominated basins, snow storage can approximate the dominant component of solid TWS. However, in glacierized basins, such as the Yukon basin in the North American Arctic, glacier mass changes may also contribute substantially to solid TWS variations. Publicly available monthly glacier mass-change products remain limited compared with SWE products, which may restrict the application of the framework in glacier-rich regions. Even within the Eurasian Arctic, uncertainties among SWE products remain substantial because of differences in forcing data, model structure, and snow-process representation. These uncertainties can propagate into both TWS and discharge reconstructions.

Second, the current framework does not explicitly represent hydrological changes associated with permafrost thaw. Recent studies have shown that permafrost degradation has contributed to the drainage and shrinkage of Arctic lowland lakes (Webb et al., 2022; Webb and Liljedahl, 2023). Because these processes are not included in the reconstruction framework, discharge changes associated with lake drainage or altered subsurface connectivity may not be fully captured. Users should therefore interpret the dataset with caution in lowland permafrost regions where surface-water storage and drainage pathways are changing rapidly.

Third, the dataset inherits the effective spatial-resolution limitation of GRACE TWS observations. In this study, discharge reconstruction was limited to gauges with contributing areas larger than 90,000 km², which excludes many smaller Arctic basins. This limitation is important because smaller river systems can also show substantial hydrological changes. Feng et al. (2021) reported that, during 1984–2018, river reaches with drainage areas smaller than 1,000 km² accounted for 82.5% of the reaches showing significant discharge trends. Future work should therefore extend natural discharge reconstruction to smaller basins by combining statistical downscaling (Gou and Soja, 2024; Li and Kusche, 2026), regional hydrological constraints, and observations from next-generation satellite gravity missions (Yan et al., 2026).

https://doi.org/10.5194/essd-2026-531
Preprint. Discussion started: 10 August 2026

6 Example applications

400 ### 6.1 Trends in annual natural discharge and apportionment entropy

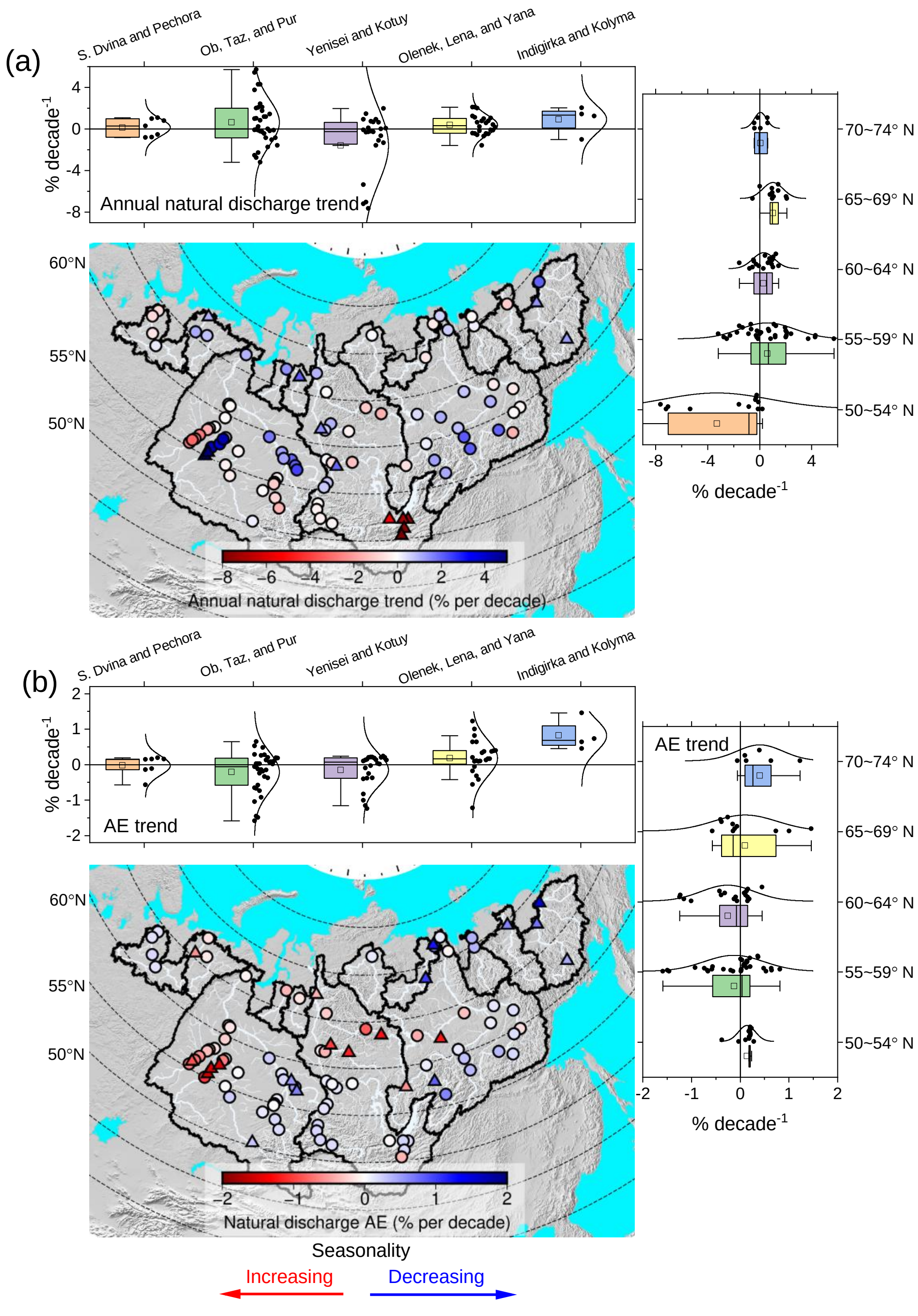

Figure 10. Sen's slope trends in reconstructed annual natural discharge and Apportionment Entropy (AE) at 94 gauges from 1953 to 2025. (a) Trends in annual natural discharge for hydrological years from September to the following August, expressed as percent per decade relative to mean annual discharge. (b) Trends in AE derived from reconstructed monthly natural discharge, expressed as percent

https://doi.org/10.5194/essd-2026-531
Preprint. Discussion started: 10 August 2026

per decade relative to mean AE. Triangles and circles denote significant ($p<0.05$) and nonsignificant trends, respectively, based on the Mann Kendall test. Boxplots above and to the right of each map summarize gauge-level trends by basin and latitude band, respectively.

Using the reconstructed natural discharge, we estimated Sen's slope trends in annual natural discharge and AE for the 1953–2025 hydrological years at 94 gauges (Figure 10). Both metrics showed substantial regional variability. The 5th–95th percentile ranges were −4.92 to 3.48% decade^{-1} for annual discharge trends and −1.21 to 0.71% decade^{-1} for AE trends. Annual natural discharge generally increased in the eastern basins, particularly the Olenek, Lena, Yana, Indigirka, and Kolyma basins. Weak or negative trends were mainly found at gauges with relatively small contributing areas in parts of the western and central basins. AE increased at 60.6% of the gauges, indicating a more even monthly distribution of discharge. In contrast, decreasing AE trends were concentrated between 55°N and 65°N in the Ob, Yenisei, and Lena basins. Annual discharge and AE trends showed different spatial patterns, indicating that changes in annual discharge magnitude were not always accompanied by corresponding changes in seasonal allocation. Despite these regional differences, neither metric showed a clear monotonic gradient with latitude.

Based on the Mann–Kendall test, significant trends were detected at 13.8% of the gauges for annual natural discharge and at 23.3% for AE. Thus, statistically detectable changes in seasonal allocation were identified at more gauges than those in annual discharge magnitude. Significant decreases in annual discharge were concentrated along the Ishim River in the Ob basin and the Selenga River in the Yenisei basin, whereas significant increases were mainly observed along the Kolyma River in the Kolyma basin. Significant AE decreases occurred along parts of the Ishim River in the Ob basin and the Podkamennaya Tunguska River in the Yenisei basin, indicating stronger seasonality. In contrast, significant AE increases in the Olenek, Indigirka, and Kolyma basins indicated weaker seasonality and a more even within-year distribution of discharge.

6.2 Effects of anthropogenic regulation at major river outlets

Hydropower reservoirs can redistribute river discharge from high-flow impoundment periods to low-flow release periods. To assess whether this regulation remains detectable far downstream, we compared discharge anomalies, calculated as observations minus reconstructions, at downstream gauges near the outlets of the Ob, Yenisei, Lena, and Kolyma rivers with the timing of upstream hydropower commissioning and initial reservoir impoundment.

During the low-flow release period (November–April of the hydrological year), discharge anomalies generally shifted toward positive values after major hydropower units became operational (Figure 11). The clearest response occurred at Igarka (ID: 43) in the Yenisei basin, where anomalies showed stepwise increases following the successive commissioning of several large upstream hydropower units and clearly exceeded the background range derived from minimally regulated gauges (Figure 11e). Kyusyur (ID: 74) in the Lena basin also showed persistent positive anomalies after the Vilyui hydropower system became operational. A weaker positive response was observed at Kolymskaya (ID: 94) in the Kolyma basin, although the shorter record limits confidence in this result. In contrast, anomalies at Salekhard (ID: 08) in the Ob basin generally remained within the background range and showed only weak correspondence with hydropower commissioning.

https://doi.org/10.5194/essd-2026-531
Preprint. Discussion started: 10 August 2026

Open Access Earth System Science Data Discussions

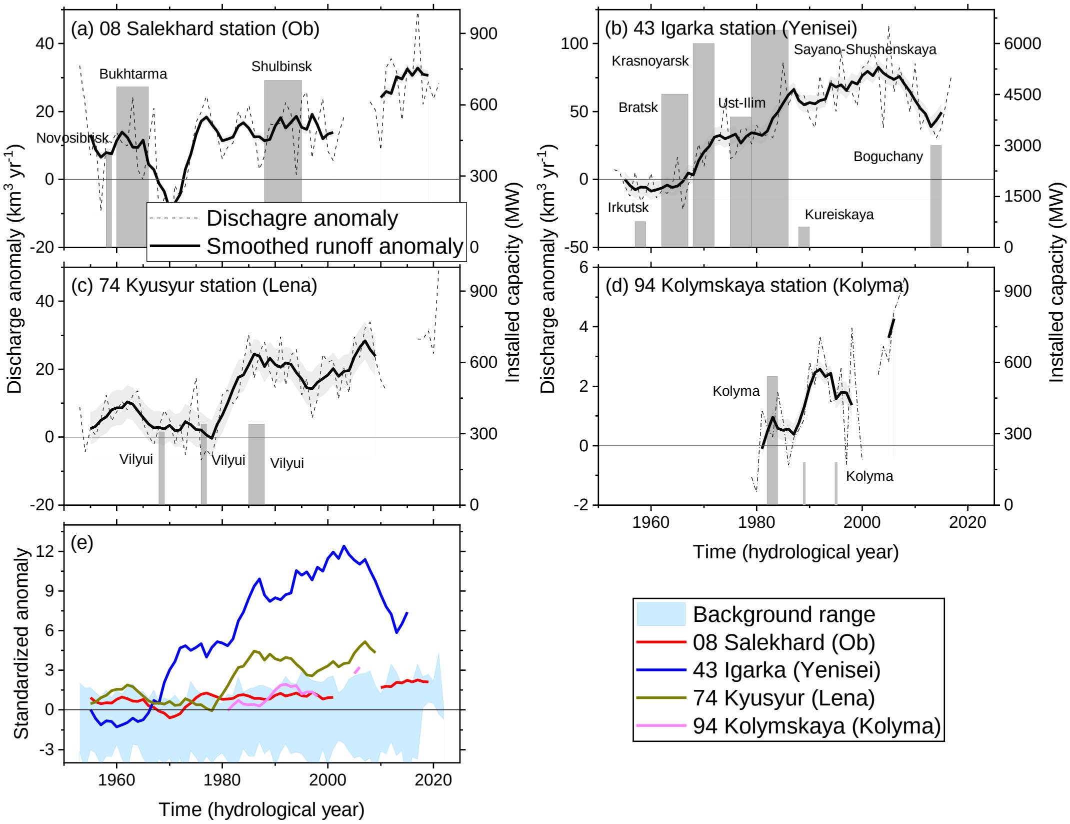

Figure 11. Discharge anomalies during the low-flow release period at downstream gauges near the outlets of major regulated Eurasian Arctic rivers and their correspondence with upstream hydropower commissioning. The low-flow release period was defined as November–April of each hydrological year, and discharge anomalies were calculated as observed minus reconstructed natural discharge. Gray bars indicate the commissioning years and installed capacities of major hydropower units. (a) Salekhard in the Ob basin (ID: 08). (b) Igarka in the Yenisei basin (ID: 43). (c) Kyusyur in the Lena basin (ID: 74). (d) Kolymskaya in the Kolyma basin (ID: 94). (e) Standardized discharge anomalies at the four regulated gauges compared with the 5th–95th percentile background range derived from 61 minimally regulated gauges. Anomalies at minimally regulated gauges were standardized by their full-period standard deviations, whereas anomalies at the four regulated gauges were standardized by the standard deviations during their training periods.

During the high-flow impoundment period (June–September of the hydrological year), negative anomalies were temporally associated with the initial filling of major upstream reservoirs (Figure 12). At Igarka, persistent negative anomalies during the filling of several large reservoirs fell well below the background range (Figure 12e), indicating that the initial impoundment of large upstream reservoirs substantially reduced warm-season discharge downstream. At Kyusyur, negative anomalies were strongest during and shortly after the initial filling of the Vilyui reservoir but later returned toward the background range, suggesting that the effect was concentrated in the initial impoundment stage. No comparably persistent signal was identified at Salekhard or Kolymskaya.

https://doi.org/10.5194/essd-2026-531
Preprint. Discussion started: 10 August 2026

Open Access Earth System Science Data Discussions

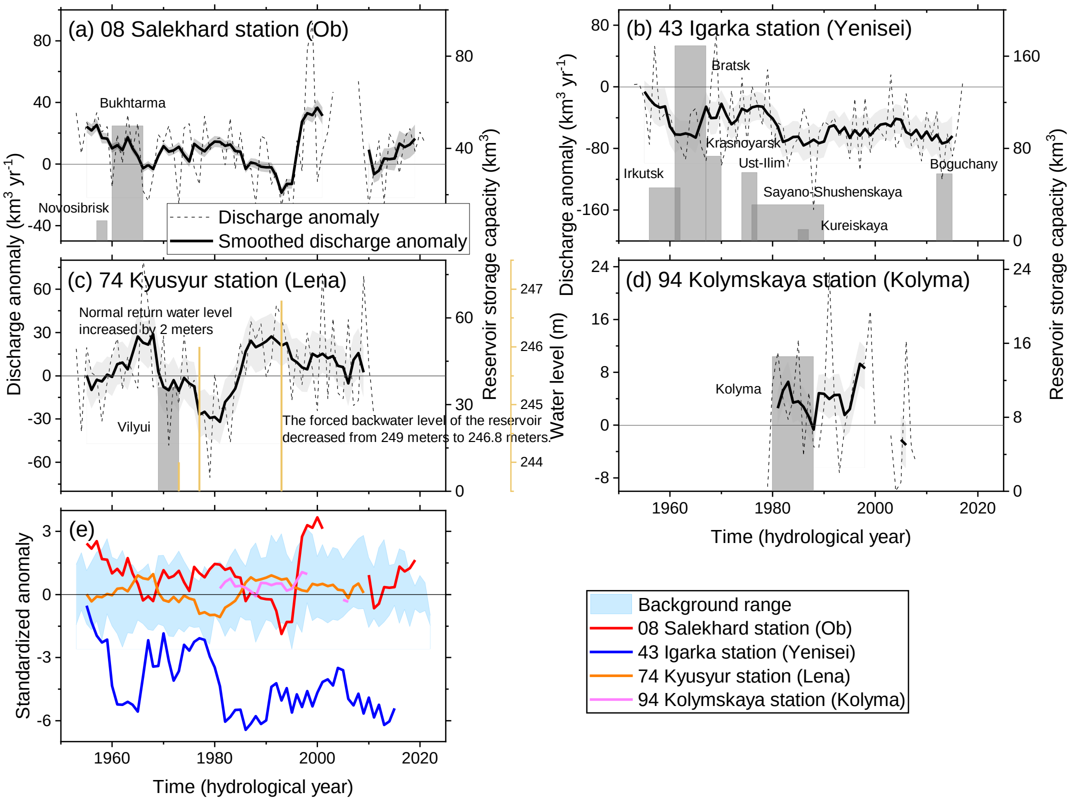

Figure 12. Discharge anomalies during the high-flow impoundment period at downstream gauges near the outlets of major regulated Eurasian Arctic rivers and their correspondence with the timing of initial upstream reservoir impoundment. The high-flow impoundment period was defined as June–September of each hydrological year, and discharge anomalies were calculated as observed minus reconstructed natural discharge. Gray bars indicate the initial impoundment periods and storage capacities of major reservoirs. (a) Salekhard in the Ob basin (ID 08). (b) Igarka in the Yenisei basin (ID 43). (c) Kyusyur in the Lena basin (ID 74). (d) Kolymskaya in the Kolyma basin (ID 94). (e) Standardized discharge anomalies at the four regulated gauges compared with the 5th–95th percentile background range derived from 61 minimally regulated gauges. Standardization followed the procedure described for Figure 11e.

The downstream effect of human regulation appears to depend on the storage capacity and installed hydropower capacity of upstream reservoirs. The strongest signal was detected in the Yenisei basin, where several large hydropower systems are located upstream of Igarka. At this gauge, observed mean annual discharge during 1960–1990 was approximately 6.85% lower than reconstructed natural discharge (Figure 5a), indicating that the initial filling of major upstream reservoirs affected the annual discharge baseline. Regulation also altered seasonal allocation. After 1960, observed AE increased by 9.78% relative to the pre-regulation mean, whereas AE derived from reconstructed natural discharge increased by only 0.15% (Figure 6a), indicating that regulation substantially weakened discharge seasonality. At Kyusyur in the Lena basin, observed AE increased by 6.22% after 1970, compared with 1.08% for reconstructed natural discharge, indicating that upstream hydropower regulation also affected seasonal discharge allocation near the river outlet. The Kolyma results suggest a possible but less certain regulation signal because of limited observations. In contrast, no clear regulatory signal was detected at Salekhard in the Ob basin under the current data and reconstruction framework, possibly because the downstream effect of upstream regulation was relatively small and partly masked by uncertainties in the reconstructed natural discharge.

https://doi.org/10.5194/essd-2026-531
Preprint. Discussion started: 10 August 2026

7 Data availability

All datasets used in this study are publicly available, and their sources are listed in Table 4. The reconstructed monthly natural discharge dataset for 94 gauging stations in the Eurasian Arctic from 1952 onward is available at https://doi.org/10.5281/zenodo.21157816 (Liu et al., 2026). The dataset is provided in both MAT and NetCDF-4 formats to facilitate reuse by different user communities and software environments.

Table 4. Data availability in this study

Production	Full Form	Link
CSR mascon		https://www2.csr.utexas.edu/grace/RL06_mascons.html
JPL mascon		https://grace.jpl.nasa.gov/data/get-data/jpl_global_mascons/
GSFC mascon		https://earth.gsfc.nasa.gov/geo/data/grace-mascons
GRDC	Global Runoff Data Centre	https://grdc.bafg.de/
CRU	Climatic Research Unit Time-series data	https://crudata.uea.ac.uk/cru/data/hrg/cru_ts_4.09
GPCC	Global Precipitation Climatology Centre data	https://www.dwd.de/EN/ourservices/gpcc/gpcc.html
BEST	Berkeley Earth Surface Temperatures	https://berkeleyearth.org/data/
U. Delaware	University of Delaware Air Temperature & Precipitation	https://psl.noaa.gov/data/gridded/data.UDel_AirT_Precip.html
WaterGAP 20crv3-w5e5	Water – Global Assessment and Prognosis	https://gude.uni-frankfurt.de/collections/61f471df-7fda-478a-a7f5-6d8ae9be0f5d
CPC	Climate Prediction Center	https://psl.noaa.gov/data/gridded/data.cpc.globalprecip.html
JRA-3Q	Japanese Reanalysis for Three Quarters of a Century	https://www.data.jma.go.jp/jra/html/JRA-3Q/index_en.html
ERA5 single	ERA5 monthly averaged data on single levels	https://cds.climate.copernicus.eu/datasets/reanalysis-era5-single-levels-monthly-means?tab=overview
GLDAS NOAH	Global Land Data Assimilation System Noah Land Surface Model	https://ldas.gsfc.nasa.gov/gldas
ERA5-land	ERA5-Land monthly averaged data	https://cds.climate.copernicus.eu/datasets/reanalysis-era5-land-monthly-means?tab=overview
Crocus-ERA5	Crocus-ERA5 snow product	https://zenodo.org/records/14513248

8 Conclusion

In this study, we present a gauge-based monthly natural discharge reconstruction dataset for 94 gauges in the Eurasian Arctic from 1952 to 2025. The dataset was generated using a basin-scale framework and evaluated using monthly and annual discharge and seasonal allocation metrics. The reconstructed natural discharge agreed well with observations at minimally regulated gauges and during the pre-regulation periods of regulated gauges, with median monthly KGE values exceeding 0.88. After summing monthly values to annual discharge, the reconstruction also captured observed variability at minimally regulated gauges, with a median annual KGE of 0.73. The reconstruction further reproduced year-to-year changes in seasonal discharge allocation, with a median AE KGE of 0.49 at minimally regulated gauges. Together, these evaluations support the reliability of the reconstructed natural discharge records.

Several limitations remain, including uncertainties in solid-water representation, the lack of explicit permafrost-related hydrological processes, and the coarse effective spatial resolution inherited from GRACE TWS observations. Nevertheless, within the Eurasian Arctic, the reconstructed gauge-based discharge records showed better agreement with gauge-based observations than discharge estimates derived from existing GRACE-like TWS products and from a gridded runoff reconstruction product. The dataset therefore provides a long-term natural-discharge baseline for characterizing changes in annual discharge and seasonal allocation over the past seven decades, and for assessing the roles of climate variability and human regulation in poorly monitored Arctic basins.

Author contributions

Bingshi Liu: Conceptualization; Data curation; Formal analysis; Funding acquisition; Investigation; Methodology; Project administration; Software; Validation; Visualization; Writing (original draft preparation); Writing (review and editing). **Xiancai Zou:** Conceptualization; Funding acquisition; Project administration; Resources; Supervision; Writing (review and editing). **Jiancheng Li:** Funding acquisition; Project administration; Resources; Supervision; Writing (review and editing). **Taoyong Jin:** Writing (review and editing).

Acknowledgements

The authors gratefully acknowledge the institutions, data centers, and platforms that provided the publicly available datasets used in this study.

Financial support

This work was supported by the National Natural Science Foundation of China [grant numbers 42388102, 42304002, 42192533]; the China Postdoctoral Science Foundation (CPSF) [grant numbers 2024T170678, 2023M732685]; the Postdoctoral Fellowship Program of CPSF [grant number GZB20230536].

Competing interests

The authors declare no conflicts of interest relevant to this study.

References

Andreadis, K. M., Coss, S. P., Durand, M., Gleason, C. J., Simmons, T. T., Tebaldi, N., Bjerklie, D. M., Brinkerhoff, C., Dudley, R. W., Gejadze, I., Larnier, K., Malaterre, P., Oubanas, H., Allen, G. H., Bates, P. D., David, C. H., Domeneghetti, A., Elmi, O., Marc, L. F., Prata De Moraes Frasson, R., Friedmann, E., Garambois, P., Gehring, J., Getirana, A., Hughes, M., Lee, J., Matte, P., Minear, J. T., Monnier, J., Muhebwa, A., Tourian, M. J., Pavelsky, T. M., Riggs, R. M., Rodríguez, E., Sikder, M. S., Smith, L. C., Stuurman, C., Taneja, J., Tarpanelli, A., Wang, J., Williams, B. A., and Yadav, B.: A First Look at River Discharge Estimation From SWOT Satellite Observations, Geophys. Res. Lett., 52, e2024GL114185, https://doi.org/10.1029/2024GL114185, 2025.

Bjerklie, D. M., Birkett, C. M., Jones, J. W., Carabajal, C., Rover, J. A., Fulton, J. W., and Garambois, P.-A.: Satellite remote sensing estimation of river discharge: Application to the Yukon River Alaska, J. Hydrol., 561, 1000–1018, https://doi.org/10.1016/j.jhydrol.2018.04.005, 2018.

Box, J. E., Colgan, W. T., Christensen, T. R., Schmidt, N. M., Lund, M., Parmentier, F.-J. W., Brown, R., Bhatt, U. S., Euskirchen, E. S., Romanovsky, V. E., Walsh, J. E., Overland, J. E., Wang, M., Corell, R. W., Meier, W. N., Wouters, B., Mernild, S., Mård, J., Pawlak, J., and Olsen, M. S.: Key indicators of Arctic climate change: 1971–2017, Environ. Res. Lett., 14, 045010, https://doi.org/10.1088/1748-9326/aafc1b, 2019.

https://doi.org/10.5194/essd-2026-531
Preprint. Discussion started: 10 August 2026

Bring, A. and Destouni, G.: Arctic Climate and Water Change: Model and Observation Relevance for Assessment and Adaptation, Surv. Geophys., 35, 853–877, https://doi.org/10.1007/s10712-013-9267-6, 2014.

Bring, A., Fedorova, I., Dibike, Y., Hinzman, L., Mård, J., Mernild, S. H., Prowse, T., Semenova, O., Stuefer, S. L., and Woo, M. -K.: Arctic terrestrial hydrology: A synthesis of processes, regional effects, and research challenges, J. Geophys. Res. Biogeosciences, 121, 621–649, https://doi.org/10.1002/2015JG003131, 2016.

Chen, J., Tapley, B., Rodell, M., Seo, K., Wilson, C., Scanlon, B. R., and Pokhrel, Y.: Basin-Scale River Runoff Estimation From GRACE Gravity Satellites, Climate Models, and In Situ Observations: A Case Study in the Amazon Basin, Water Resour. Res., 56, e2020WR028032, https://doi.org/10.1029/2020WR028032, 2020.

Chen, M., Shi, W., Xie, P., Silva, V. B. S., Kousky, V. E., Wayne Higgins, R., and Janowiak, J. E.: Assessing objective techniques for gauge-based analyses of global daily precipitation, J. Geophys. Res. Atmospheres, 113, 2007JD009132, https://doi.org/10.1029/2007JD009132, 2008.

Coss, S., Durand, M., Yi, Y., Jia, Y., Guo, Q., Tuozzolo, S., Shum, C. K., Allen, G. H., Calmant, S., and Pavelsky, T.: Global River Radar Altimetry Time Series (GRRATS): new river elevation earth science data records for the hydrologic community, Earth Syst. Sci. Data, 12, 137–150, https://doi.org/10.5194/essd-12-137-2020, 2020.

Feng, D., Gleason, C. J., Lin, P., Yang, X., Pan, M., and Ishitsuka, Y.: Recent changes to Arctic river discharge, Nat. Commun., 12, 6917, https://doi.org/10.1038/s41467-021-27228-1, 2021.

Feng, D., Yang, X., Pavelsky, T. M., Allen, G. H., Bates, P., Gleason, C. J., Gardner, J., Lehner, B., Wang, J., Cooley, S., Tarpanelli, A., Battin, T., Yamazaki, D., Durand, M., Raymond, P., Boothroyd, R., Lin, P., and Andreadis, K. M.: Remote sensing and the new global river science, Nat. Water, https://doi.org/10.1038/s44221-026-00665-2, 2026.

Gentner, L. Q., Gou, J., Tourian, M. J., Börger, L., Sneeuw, N., and Soja, B.: DeepRec: Global Terrestrial Water Storage Reconstruction Since 1941 Using Spatiotemporal-Aware Deep Learning Model, J. Geophys. Res. Mach. Learn. Comput., 3, e2025JH000889, https://doi.org/10.1029/2025JH000889, 2026.

Ghiggi, G., Humphrey, V., Seneviratne, S. I., and Gudmundsson, L.: GRUN: an observation-based global gridded runoff dataset from 1902 to 2014, Earth Syst. Sci. Data, 11, 1655–1674, https://doi.org/10.5194/essd-11-1655-2019, 2019.

Gleason, C. J. and Smith, L. C.: Toward global mapping of river discharge using satellite images and at-many-stations hydraulic geometry, Proc. Natl. Acad. Sci., 111, 4788–4791, https://doi.org/10.1073/pnas.1317606111, 2014.

Gou, J. and Soja, B.: Global high-resolution total water storage anomalies from self-supervised data assimilation using deep learning algorithms, Nat. Water, 2, 139–150, https://doi.org/10.1038/s44221-024-00194-w, 2024.

Gudmundsson, L., Brunner, M. I., Döll, P., Fluet-Chouinard, E., Frolova, N., Gosling, S. N., Hirabayashi, Y., Kireeva, M. B., Liu, X., Müller Schmied, H., Magritskiy, D., Slater, L. J., Stein, L., Tramblay, Y., Wang, K., Wasko, C., Yamazaki, D., and Zhou, X.: Past and future change in global river flows, Nat. Rev. Earth Environ., 7, 7–23, https://doi.org/10.1038/s43017-025-00745-z, 2025.

Hacker, C., Gutknecht, B. D., LÃ¶cher, A., and Kusche, J.: Multidecadal reconstruction of terrestrial water storage changes by combining pre-GRACE satellite observations and climate data, Earth Syst. Sci. Data, 18, 1747–1781, https://doi.org/10.5194/essd-18-1747-2026, 2026.

Harris, I., Osborn, T. J., Jones, P., and Lister, D.: Version 4 of the CRU TS monthly high-resolution gridded multivariate climate dataset, Sci. Data, 7, 109, https://doi.org/10.1038/s41597-020-0453-3, 2020.

Hersbach, H., Bell, B., Berrisford, P., Hirahara, S., Horányi, A., Muñoz-Sabater, J., Nicolas, J., Peubey, C., Radu, R., Schepers, D., Simmons, A., Soci, C., Abdalla, S., Abellan, X., Balsamo, G., Bechtold, P., Biavati, G., Bidlot, J., Bonavita, M., De Chiara, G., Dahlgren, P., Dee, D., Diamantakis, M., Dragani, R., Flemming, J., Forbes, R., Fuentes, M., Geer, A., Haimberger, L., Healy, S., Hogan, R. J., Hólm, E., Janisková, M., Keeley, S., Laloyaux, P., Lopez, P., Lupu, C., Radnoti, G., De Rosnay, P., Rozum, I., Vamborg, F., Villaume, S., and Thépaut, J.: The ERA5 global reanalysis, Q. J. R. Meteorol. Soc., 146, 1999–2049, https://doi.org/10.1002/qj.3803, 2020.

Hirschi, M., Stradiotti, P., Crezee, B., Dorigo, W., and Seneviratne, S. I.: Potential of long-term satellite observations and reanalysis products for characterising soil drying: trends and drought events, Hydrol. Earth Syst. Sci., 29, 397–425, https://doi.org/10.5194/hess-29-397-2025, 2025.

Holmes, R. M.: NOAA Arctic Report Card 2021: River Discharge, NOAA Tech. Rep. OAR ARC 21-11, https://doi.org/10.25923/ZEVF-AR65, 2021.

Humphrey, V. and Gudmundsson, L.: GRACE-REC: a reconstruction of climate-driven water storage changes over the last century, Earth Syst. Sci. Data, 11, 1153–1170, https://doi.org/10.5194/essd-11-1153-2019, 2019.

Jennings, K. S., Winchell, T. S., Livneh, B., and Molotch, N. P.: Spatial variation of the rain–snow temperature threshold across the Northern Hemisphere, Nat. Commun., 9, 1148, https://doi.org/10.1038/s41467-018-03629-7, 2018.

Jones, B. M., Grosse, G., Farquharson, L. M., Roy-Léveillée, P., Veremeeva, A., Kanevskiy, M. Z., Gaglioti, B. V., Breen, A. L., Parsekian, A. D., Ulrich, M., and Hinkel, K. M.: Lake and drained lake basin systems in lowland permafrost regions, Nat. Rev. Earth Environ., 3, 85–98, https://doi.org/10.1038/s43017-021-00238-9, 2022.

Kosaka, Y., Kobayashi, S., Harada, Y., Kobayashi, C., Naoe, H., Yoshimoto, K., Harada, M., Goto, N., Chiba, J., Miyaoka, K., Sekiguchi, R., Deushi, M., Kamahori, H., Nakaegawa, T., Tanaka, T. Y., Tokuhiro, T., Sato, Y., Matsushita, Y., and Onogi, K.: The JRA-3Q Reanalysis, J. Meteorol. Soc. Jpn. Ser II, 102, 49–109, https://doi.org/10.2151/jmsj.2024-004, 2024.

Lauer, M., Rinke, A., Gorodetskaya, I., Sprenger, M., Mech, M., and Crewell, S.: Influence of atmospheric rivers and associated weather systems on precipitation in the Arctic, Atmospheric Chem. Phys., 23, 8705–8726, https://doi.org/10.5194/acp-23-8705-2023, 2023.

Lehner, B., Beames, P., Mulligan, M., Zarfl, C., De Felice, L., Van Soesbergen, A., Thieme, M., Garcia De Leaniz, C., Anand, M., Belletti, B., Brauman, K. A., Januchowski-Hartley, S. R., Lyon, K., Mandle, L., Mazany-Wright, N., Messager, M. L., Pavelsky, T., Pekel, J.-F., Wang, J., Wen, Q., Wishart, M., Xing, T., Yang, X., and Higgins, J.: The Global Dam Watch database of river barrier and reservoir information for large-scale applications, Sci. Data, 11, 1069, https://doi.org/10.1038/s41597-024-03752-9, 2024.

Leopardi, F., Dari, J., Saltalippi, C., Brocca, L., Volden, E., Fernández-Prieto, D., Saemian, P., Sneeuw, N., Tourian, M. J., and Camici, S.: A satellite-based approach for estimating runoff and river discharge in the Pan-Arctic region from 2003 to 2022, Remote Sens. Environ., 338, 115353, https://doi.org/10.1016/j.rse.2026.115353, 2026.

Li, F. and Kusche, J.: Reproducing GRACE Total Water Storage Change at Finer Spatial Scales, Geophys. Res. Lett., 53, e2025GL119881, https://doi.org/10.1029/2025GL119881, 2026.

Li, F., Kusche, J., Chao, N., Wang, Z., and Löcher, A.: Long-Term (1979-Present) Total Water Storage Anomalies Over the Global Land Derived by Reconstructing GRACE Data, Geophys. Res. Lett., 48, e2021GL093492, https://doi.org/10.1029/2021GL093492, 2021.

Lin, P., Pan, M., Beck, H. E., Yang, Y., Yamazaki, D., Frasson, R., David, C. H., Durand, M., Pavelsky, T. M., Allen, G. H., Gleason, C. J., and Wood, E. F.: Global Reconstruction of Naturalized River Flows at 2.94 Million Reaches, Water Resour. Res., 55, 6499–6516, https://doi.org/10.1029/2019WR025287, 2019.

Liu, B., Zou, X., Yi, S., Sneeuw, N., Cai, J., and Li, J.: Identifying and separating climate- and human-driven water storage anomalies using GRACE satellite data, Remote Sens. Environ., 263, 112559, https://doi.org/10.1016/j.rse.2021.112559, 2021.

Liu, B., Zou, X., Yi, S., Sneeuw, N., Li, J., and Cai, J.: Reconstructing GRACE-like time series of high mountain glacier mass anomalies, Remote Sens. Environ., 280, 113177, https://doi.org/10.1016/j.rse.2022.113177, 2022.

Liu, B., Zou, X., Li, J., and Jin, T.: Monthly Natural Discharge Reconstruction for 94 Eurasian Arctic Gauges, 1952–2025, https://doi.org/10.5281/ZENODO.21157816, 3 July 2026.

Loomis, B. D., Luthcke, S. B., and Sabaka, T. J.: Regularization and error characterization of GRACE mascons, J. Geod., 93, 1381–1398, https://doi.org/10.1007/s00190-019-01252-y, 2019.

Luthcke, S. B., Sabaka, T. J., Loomis, B. D., Arendt, A. A., McCarthy, J. J., and Camp, J.: Antarctica, Greenland and Gulf of Alaska land-ice evolution from an iterated GRACE global mascon solution, J. Glaciol., 59, 613–631, https://doi.org/10.3189/2013JoG12J147, 2013.

Müller Schmied, H., Trautmann, T., Ackermann, S., Cáceres, D., Flörke, M., Gerdener, H., Kynast, E., Peiris, T. A., Schiebener, L., Schumacher, M., and Döll, P.: The global water resources and use model WaterGAP v2.2e: description and evaluation of modifications and new features, Geosci. Model Dev., 17, 8817–8852, https://doi.org/10.5194/gmd-17-8817-2024, 2024.

Muñoz-Sabater, J., Dutra, E., Agustí-Panareda, A., Albergel, C., Arduini, G., Balsamo, G., Boussetta, S., Choulga, M., Harrigan, S., Hersbach, H., Martens, B., Miralles, D. G., Piles, M., Rodríguez-Fernández, N. J., Zsoter, E., Buontempo, C., and Thépaut, J.-N.: ERA5-Land: a state-of-the-art global reanalysis dataset for land applications, Earth Syst. Sci. Data, 13, 4349–4383, https://doi.org/10.5194/essd-13-4349-2021, 2021.

Peterson, B. J., Holmes, R. M., McClelland, J. W., Vörösmarty, C. J., Lammers, R. B., Shiklomanov, A. I., Shiklomanov, I. A., and Rahmstorf, S.: Increasing River Discharge to the Arctic Ocean, Science, 298, 2171–2173, https://doi.org/10.1126/science.1077445, 2002.

Ramos Buarque, S., Decharme, B., Barbu, A. L., and Franchisteguy, L.: Insights into the North Hemisphere daily snowpack at high resolution from the new Crocus–ERA5 product, Earth Syst. Sci. Data, 17, 7227–7249, https://doi.org/10.5194/essd-17-7227-2025, 2025.

Riegger, J. and Tourian, M. J.: Characterization of runoff-storage relationships by satellite gravimetry and remote sensing, Water Resour. Res., 50, 3444–3466, https://doi.org/10.1002/2013WR013847, 2014.

Rodell, M. and Reager, J. T.: Water cycle science enabled by the GRACE and GRACE-FO satellite missions, Nat. Water, 1, 47–59, https://doi.org/10.1038/s44221-022-00005-0, 2023.

Rodell, M., Houser, P. R., Jambor, U., Gottschalck, J., Mitchell, K., Meng, C.-J., Arsenault, K., Cosgrove, B., Radakovich, J., Bosilovich, M., Entin, J. K., Walker, J. P., Lohmann, D., and Toll, D.: The Global Land Data Assimilation System, Bull. Am. Meteorol. Soc., 85, 381–394, https://doi.org/10.1175/BAMS-85-3-381, 2004.

Rohde, R. A. and Hausfather, Z.: The Berkeley Earth Land/Ocean Temperature Record, Earth Syst. Sci. Data, 12, 3469–3479, https://doi.org/10.5194/essd-12-3469-2020, 2020.

Save, H., Bettadpur, S., and Tapley, B. D.: High-resolution CSR GRACE RL05 mascons, J. Geophys. Res. Solid Earth, 121, 7547–7569, https://doi.org/10.1002/2016JB013007, 2016.

Scherer, D., Schwatke, C., Dettmering, D., and Seitz, F.: Monitoring river discharge from space: An optimization approach with uncertainty quantification for small ungauged rivers, Remote Sens. Environ., 315, 114434, https://doi.org/10.1016/j.rse.2024.114434, 2024.

Schirmeister, Z., Finger, P., Rustemeier, E., and Ziese, M.: GPCC Precipitation Analysis Monthly Version 2025 (at 0.25°, 0.5°, 1.0°, 2.5°) (2025), https://doi.org/10.5676/DWD_GPCC/MONTHLY_V2025_050, 2025.

Shiklomanov, A. I., Lammers, R. B., and Vörösmarty, C. J.: Widespread decline in hydrological monitoring threatens Pan-Arctic Research, Eos Trans. Am. Geophys. Union, 83, 13–17, https://doi.org/10.1029/2002EO000007, 2002.

Sneeuw, N., Lorenz, C., Devaraju, B., Tourian, M. J., Riegger, J., Kunstmann, H., and Bárdossy, A.: Estimating Runoff Using Hydro-Geodetic Approaches, Surv. Geophys., 35, 1333–1359, https://doi.org/10.1007/s10712-014-9300-4, 2014.

Tapley, B. D., Watkins, M. M., Flechtner, F., Reigber, C., Bettadpur, S., Rodell, M., Sasgen, I., Famiglietti, J. S., Landerer, F. W., Chambers, D. P., Reager, J. T., Gardner, A. S., Save, H., Ivins, E. R., Swenson, S. C., Boening, C., Dahle, C., Wiese, D. N., Dobslaw, H., Tamisiea, M. E., and Velicogna, I.: Contributions of GRACE to understanding climate change, Nat. Clim. Change, 9, 358–369, https://doi.org/10.1038/s41558-019-0456-2, 2019.

Tiwari, A. D., Pokhrel, Y., Boulange, J., Burek, P., Guillaumot, L., Gosling, S. N., Grillakis, M., Hanasaki, N., Koutroulis, A., Ostberg, S., Otta, K., Schmied, H. M., Satoh, Y., Scanlon, B., Stacke, T., and Yokohata, T.: Similarities and divergent patterns in hydrologic fluxes and storages simulated by global water models, Nat. Water, 3, 550–560, https://doi.org/10.1038/s44221-025-00435-6, 2025.

https://doi.org/10.5194/essd-2026-531
Preprint. Discussion started: 10 August 2026

Vinogradova, N. T., Pavelsky, T. M., Farrar, J. T., Hossain, F., and Fu, L.-L.: A new look at Earth's water and energy with SWOT, Nat. Water, 3, 27–37, https://doi.org/10.1038/s44221-024-00372-w, 2025.

Watkins, M. M., Wiese, D. N., Yuan, D., Boening, C., and Landerer, F. W.: Improved methods for observing Earth's time variable mass distribution with GRACE using spherical cap mascons, J. Geophys. Res. Solid Earth, 120, 2648–2671, https://doi.org/10.1002/2014JB011547, 2015.

Webb, E. E. and Liljedahl, A. K.: Diminishing lake area across the northern permafrost zone, Nat. Geosci., 16, 202–209, https://doi.org/10.1038/s41561-023-01128-z, 2023.

Webb, E. E., Liljedahl, A. K., Cordeiro, J. A., Loranty, M. M., Witharana, C., and Lichstein, J. W.: Permafrost thaw drives surface water decline across lake-rich regions of the Arctic, Nat. Clim. Change, 12, 841–846, https://doi.org/10.1038/s41558-022-01455-w, 2022.

White, D., Hinzman, L., Alessa, L., Cassano, J., Chambers, M., Falkner, K., Francis, J., Gutowski, W. J., Holland, M., Holmes, R. M., Huntington, H., Kane, D., Kliskey, A., Lee, C., McClelland, J., Peterson, B., Rupp, T. S., Straneo, F., Steele, M., Woodgate, R., Yang, D., Yoshikawa, K., and Zhang, T.: The arctic freshwater system: Changes and impacts, J. Geophys. Res. Biogeosciences, 112, 2006JG000353, https://doi.org/10.1029/2006JG000353, 2007.

Wiese, D. N., Landerer, F. W., and Watkins, M. M.: Quantifying and reducing leakage errors in the JPL RL05M GRACE mascon solution, Water Resour. Res., 52, 7490–7502, https://doi.org/10.1002/2016WR019344, 2016.

Willmott, C. J. and Matsuura, K.: Smart Interpolation of Annually Averaged Air Temperature in the United States, J. Appl. Meteorol., 34, 2577–2586, https://doi.org/10.1175/1520-0450(1995)034%3C2577:SIOAAA%3E2.0.CO;2, 1995.

Winkelbauer, S., Mayer, M., Seitner, V., Zsoter, E., Zuo, H., and Haimberger, L.: Diagnostic evaluation of river discharge into the Arctic Ocean and its impact on oceanic volume transports, Hydrol. Earth Syst. Sci., 26, 279–304, https://doi.org/10.5194/hess-26-279-2022, 2022.

Xie, P. and Yi, S.: Reconstruction of climate-driven global terrestrial water storage variations (2002–2021) using a four-parameter linear recursive model, Hydrol. Earth Syst. Sci., 30, 3221–3244, https://doi.org/10.5194/hess-30-3221-2026, 2026.

Xie, P., Chen, M., Yang, S., Yatagai, A., Hayasaka, T., Fukushima, Y., and Liu, C.: A Gauge-Based Analysis of Daily Precipitation over East Asia, J. Hydrometeorol., 8, 607–626, https://doi.org/10.1175/JHM583.1, 2007.

Yan, Z., Ran, J., Chen, J., Lasser, M., Smith, P., Zhang, Y., and Massotti, L.: Breaking the Temporal Resolution Barrier: Projected Performance of Hybrid Gravity Satellite Ensemble by the Early 2030s, Earths Future, 14, e2025EF006825, https://doi.org/10.1029/2025EF006825, 2026.

Yi, S., Saemian, P., Sneeuw, N., and Tourian, M. J.: Estimating runoff from pan-Arctic drainage basins for 2002–2019 using an improved runoff-storage relationship, Remote Sens. Environ., 298, 113816, https://doi.org/10.1016/j.rse.2023.113816, 2023.

Yin, J., Slater, L. J., Khouakhi, A., Yu, L., Liu, P., Li, F., Pokhrel, Y., and Gentine, P.: GTWS-MLrec: global terrestrial water storage reconstruction by machine learning from 1940 to present, Earth Syst. Sci. Data, 15, 5597–5615, https://doi.org/10.5194/essd-15-5597-2023, 2023.

Zakharova, E., Nielsen, K., Kamenev, G., and Kouraev, A.: River discharge estimation from radar altimetry: Assessment of satellite performance, river scales and methods, J. Hydrol., 583, 124561, https://doi.org/10.1016/j.jhydrol.2020.124561, 2020.

Zhang, Y., Blöschl, G., Wei, H., Kong, D., Ma, N., Wagener, T., Tian, J., Xia, J., Li, C., Wang, L., Chiew, F. H. S., Leung, L. R., Liu, X., Zheng, H., Zhang, X., and Liu, C.: Overestimation of past and future increases in global river flow by Earth system models, Nat. Geosci., https://doi.org/10.1038/s41561-025-01897-9, 2026.